The three-dimensional representation of the ELF isosurface for methyl acetate (top) and sections corresponding to the planes drawn as well as to those parallel to the plane through the carbonyl group uncover many details about the distribution of electron density and can therefore contribute to supporting qualitative concepts and models. This is true not only for molecules but also for solids.

ELF: The Electron Localization Function**

Andreas Savin,* Reinhard Nesper,* Steffen Wengert, and Thomas F. Fässler

Dedicated to Professor Hans Georg von Schnering

The chemical bond is always considered from different points of view, depending on the classes of compounds or on the chemical and physical aspects to be examined. In both cases, descriptions of the chemical bond are chosen that are appropriate for the particular research or application. Therefore, there are significant differences in the understanding as what constitutes chemical bonding. This is acceptable in practice but proves to be a hindrance for true interdisciplinarity. The concept of the chemical bond offers a firm basis upon which to forge links not only within chemistry but also to all related sciences. The general desire and the growing necessity for interdisciplinary collaboration requires a careful treatment of these concepts and, if possible, a tightening and standardization to a level that is widely acceptable and beneficial. In the age of tremendously fast development of computers and computer science, we believe that the electron localization function (ELF) provides a new description of the chemical bond for almost all classes of compounds. Its graphical language earns it the ultimate qualification for enhanced interdisciplinarity.

Keywords: bond theory · electron localization function · structure elucidation

1. The Electron Localization Function—ELF

Chemistry—as we know it—without the Pauli principle is inconceivable. This principle is deeply rooted in so many chemical concepts that the connection is frequently neglected; for instance, the systematics of the periodic table, steric hindrance, and the covalent bond. The Pauli principle itself is also presented in various ways. In books on quantum mechanics it is often described as a property of the wave function, which needs to be antisymmetric with respect to interchange of electrons. From textbooks on chemistry one recalls mostly the fact that orbitals can be occupied by at most two electrons. The Pauli principle is reflected in the expression for the total energy of a system both in an energy-lowering part (the exchange term) and a larger energy-raising contribution, which can be found indirectly in the kinetic energy. The following explanation is usually used: The energetically higher canonical orbitals occupy the same space as the ones lower in energy but they must have additional nodal planes (in order to meet the criterion of orthogonality) and therefore a steeper behavior. Their appearance strongly resembles a growing precipitous landscape. The slope is expressed mathematically by the derivative; the latter can be found in the formula for the kinetic energy T [Eq. (1)], where φ_i are the orbitals and n_i their occupation numbers.

$$T = \int \frac{1}{2} \sum_i n_i |\nabla \varphi_i|^2 d^3 r \tag{1}$$

The Pauli principle has been used as a basis for the explanation of many chemical concepts. For example, Gillespie's explanation of his rules.[1] In this article we will show that most of these chemical concepts can be described very well with the electron localization function (ELF). The relationship of ELF with older concepts will be emphasized first.

Artmann was the first to introduce a formulation similar in concept to ELF.[2] In quantum mechanics, the sum of squares of the N-particle wave function corresponds to a probability density. Therefore he searched for the maximum of this quantity and found it to occur where the chemist imagines the bonds; for instance, in the case of the methane molecule, he observed four valence electron pairs arranged tetrahedrally around the carbon atom.[*] Examinations of the sum of the squares of the wave function are quite interesting but difficult to perform in practice (see for example ref. [3]). Lennard-Jones recognized that only two electrons of equal spin and therefore only two coordinates

[*] Priv.-Doz. A. Savin
Université Pierre et Marie Curie
Tour 22, Couloir 22-23
4 Place Jussien, F-75252 Paris (France)
e-mail : Andreas.Savin@lct.jussieu.fr

Prof. Dr. R. Nesper, Dr. T. F. Fässler, Dr. S. Wengert
Laboratorium für Anorganische Chemie
Eidgenössische Technische Hochschule
Universitätstrasse 6, CH-8092 Zürich (Switzerland)
Fax.: Int. code +(1)632-1149
e-mail : nesper@inorg.chem.ethz.ch

[*] Artmann used an approximate valence electron wave function composed of hybrid orbitals.

are necessary for the examination of the Pauli principle, a significant simplification on the work of Artmann. Lennard-Jones found that space is divided into regions according to the Pauli principle. If an electron resides in a given region, the other stays away from that region. More precisely, if an electron resides at a place $\vec{r}$, the probability of finding an electron in the surrounding region $B(\vec{r})$ is clearly diminished. B remains practically unchanged as long as $\vec{r}$ stays in that region. The interaction of all particles under the condition of energetic stability defines the division into regions and is therefore always dependent on the system.

Even electrons with opposite spin avoid each other. This fact cannot be attributed to the Pauli principle and the effect is usually smaller by an order of magnitude. This is the reason why a given electron permits the presence of another with opposite spin in its region: the region is therefore occupied by a pair of electrons. Such a formation of pair regions corresponds exactly to the picture proposed by Kossel eighty years ago.[4]

Lennard-Jones went one step further in assigning every pair region a localized orbital. Such orbitals have only very small values outside their assigned regions. Sometimes they are denoted "chemical orbitals" because of their proximity to chemical definitions based on electron pairs (bond, lone pair of electrons) and therefore they are very useful. In addition, they can be used in the calculation of measurable quantities on equal footing with the common (delocalized, canonical) orbitals. The symmetry behavior of localized orbitals is different from that of canonical orbitals. By applying a symmetry operation, the latter (in the absence of degeneracy) always transform into themselves (except for the sign), whereas the former may be interchanged. In the ethene molecule the canonical (σ, π) orbitals are frequently considered. Their linear combination yields two equivalent localized orbitals often regarded as the C–C "banana bonds", which are interchanged upon reflection in the atomic plane.[*] The generation of localized orbitals can be problematic in symmetry groups allowing degeneracy: In practice just a minimal numeric effect can determine the localization. This can be seen, for example, in the benzene molecule[5] in which nine (six σ and three π) electron pairs are available. On the other hand it

[*] There are also localized orbitals that correspond to the C–H bonds and the 1s cores; they are interchanged for example upon inversion.

Andreas Savin was born in 1950 in Bukarest, Romania, where he studied chemistry and received his diploma in 1973. He completed his PhD thesis in 1983 under the supervision of Professor H. Preuss at the Universität Stuttgart, where he also performed his habilitation. Between 1983 and 1993 he worked at the Universität

A. Savin   R. Nesper   S. Wengert   T. F. Fässler

Stuttgart, where he also lectured from 1985 onwards, and at the Max-Planck-Institut für Festkörperforschung. In 1993 he moved to the Centre National de la Recherche Scientifique in Paris. Since 1995 he has lectured at the Université Pierre et Marie Curie, Paris. His main areas of interest are density functional theory and the electron localization function as well as Monte-Carlo procedures and the application of quantum chemical methods.

Reinhard Nesper, born in Elze/Hannover, Germany, in 1949, studied chemistry at the Universität Münster and then moved to the Max-Planck-Institut für Festkörperforschung in Stuttgart where he received his PhD thesis under the supervision of Professor von Schnering. Apart from a period of research with Professor Roald Hoffmann at Cornell University in 1984, he was a member of the scientific staff at the Max-Planck-Institut Stuttgart from 1978 to 1990. In 1989 he received his habilitation at the Universität Stuttgart and in 1990 he accepted the chair of inorganic chemistry at the ETH Zürich. His main areas of interest are solid-state chemistry, structure determination, and the electronic structure of solids as well as new materials, nanostructures, structure–property relationships, and models for structure formation.

Steffen Wengert was born in Heilbronn, Germany, in 1964. He studied chemistry at the Universität Stuttgart where he also carried out his diploma thesis in theoretical chemistry. He then moved to the ETH Zürich to work with Professor Nesper and subsequently completed his PhD thesis on the topic of "experimental and theoretical solutions to fundamental problems in Zintl compounds" in spring 1997.

Thomas F. Fässler, born in Bad Waldsee/Reute, Germany, in 1959, studied chemistry and mathematics in Konstanz. In 1988 he received his PhD for work on transition metal cluster compounds under the supervision of Professor G. Huttner in Heidelberg. During a period of research at the University of Chicago with Professor J. Burdett he carried out fundamental theoretical studies on chemical bonding at metal surfaces. Since 1991 he has been carrying out work at the ETH Zürich towards his habilitation. His research interests are focused at the interface between molecular and solid-state chemistry, and involve the synthesis, structural characterization, and the study of the electronic properties of soluble Zintl ions, Zintl phases, and intermetallic compounds.

is not possible to generate nine equivalent regions on the six-membered ring (this is only compatible with three- or ninefold rotation axes, not with a sixfold axis). A similar situation arises for clusters such as the cage of $[B_6H_6]^{2-}$ in which seven pairs of electrons are available, which is incompatible with the icosahedral symmetry of the anion. Unfortunately, this problem appears frequently in solid phases.

The homogeneous electron gas represents an extreme case. Here, the pair region must also show a translational invariancy due to the translational symmetry of the Hamiltonian operator. To understand this phenomenon the analogy to resonance structures is quite helpful. Here, the best compromise is an average of the extreme cases.

Therefore, we will return to the original treatment by Lennard-Jones. He reduced the probability density of two electrons mathematically upon integrating over all coordinates of the remaining $N - 2$ electrons. The resulting quantity (the pair density) is a function of the coordinates of two electrons, a six-dimensional function that is too complicated for our three-dimensional concept of the chemical bond that we want to develop here. A possible solution is to reduce the examination to a single electron, that is to consider the electron density. Its partitioning into contributions from different atomic orbitals is very common. The latter are not precise in the original formulation (Mulliken population analysis[6]) leading to a certain arbitrariness, which can be restricted by additional regulations such as those introduced by Davidson or Ahlrichs and co-workers.[7, 8] An additional variant is obtained by the use of "natural" bonding orbitals.[9] Bonding relationships are also discussed in terms of differences between molecule (or crystal) densities and those of atoms and ions. Nowadays, spherical atoms,[10] formerly used as a reference, can be substituted by nonspherical ones.[11] Finally, the elegant procedure of Bader and co-workers with no reference systems at all should be mentioned: only the density ρ as a function of the positional coordinates and their derivatives is used.[12] The Pauli principle can, of course, be found in the electron density, which is certainly different for bosons at a given potential. A clear connection is not easily discernible. For that reason we return to the pair density for the moment.

A solution, and at the same time a direct precursor to the electron localization function described in this article, was found by Luken and Culbertson.[13] They studied the modification of the region $B(\vec{r})$ upon substituting the point $\vec{r}$ by a neighboring point. It is small in the pair region, but becomes predominant on leaving the region (cf. the investigations of Lennard-Jones) and, as a consequence, these changes can serve in the determination of the borders of the pair region. An overlap integral is used to measure the change.

Becke and Edgecombe proposed the examination of the Taylor expansion.[14] They used the fact that for small distances $s = |\vec{r} - \vec{r}'|$ only the second derivative of the pair density P (spherically averaged around $\vec{r}$) for electrons of equal spin is important [Eq. (2)] and therefore the examination can be restricted to the value $C(\vec{r})$ which is dependent on $\vec{r}$.

$$P(\vec{r},s) = \frac{1}{2}s^2\,C(\vec{r}) + \ldots \tag{2}$$

The simplest form of a wave function satisfying the Pauli principle, is the Slater determinant. In this case C can be ex-

pressed by Equation (3); thus, the electron density [Eq. (4)] as well as the sum $\sum_i n_i |\nabla\varphi_i|^2$ over the orbitals φ_i at $\vec{r}$ can be calculated.

$$C(\vec{r}) = \frac{1}{2}\sum_i n_i |\nabla\varphi_i|^2 - \frac{1}{8}\frac{|\nabla\rho|^2}{\rho} \tag{3}$$

$$\rho = \sum_i n_i |\varphi_i|^2 \tag{4}$$

Becke and Edgecombe proposed two additional scaling rules:
1. The homogenous electron gas is used as a reference. In this system, C depends only on the electron density [Eq. (5)].

$$C(\vec{r}) \rightarrow C_h(\vec{r}) \sim \rho^{5/3} \tag{4}$$

2. The introduction of a value which is defined between zero and one. Whereas this second scaling is convenient for comparison of numerical data, it does not play a decisive role (see Sections 2–6).

Becke and Edgecombe named the scaled function the *electron localization function* (ELF) [Eq. (6)]. ELF has its highest

$$ELF = \left\{1 + \left[\frac{C(\vec{r})}{C_h(\rho(\vec{r}))}\right]^2\right\}^{-1} \tag{6}$$

value ($\rightarrow 1$) if $\vec{r}$ is within the pair region (where P does not change very much and C is small). On the other hand, ELF is small when $\vec{r}$ is close to the border between two pair regions.[15] In a homogeneous electron gas ELF has everywhere the value $1/2$.

In solid-state physics the homogeneous electron gas is commonly used as a reference system. Another reason is the aforementioned average of extreme cases, which occurs in homogenous systems leading to an average picture. The value C_h can also be introduced independently from the homogeneous electron gas.[16] Instead of a Taylor expansion, Dobson proposed the integration over a small sphere,[17] leading to the number of electrons of equal spin in the surrounding of the reference electron. Thus, Equation (2) changes to give Equation (7).

$$\int_0^R \frac{1}{2}s^2 C(\vec{r})4\pi s^2\,ds + \ldots = \frac{1}{2}\frac{4\pi R^5}{5}C(\vec{r}) + \ldots \tag{7}$$

The radius of the spheres can be made position dependent, which keeps the number of reference electrons in a sphere with radius R unchanged. Equation (8) is valid for small spheres

$$\int_{V_{sphere}} \rho(\vec{r}+\vec{s})\,d^3s \approx \rho(\vec{r})\frac{4\pi R^3}{3} + \ldots \tag{8}$$

around $\vec{r}$, where $R \sim \rho^{-1/3}$ and the number of electrons around the reference electron [see Eq. (7)] is proportional to $C(\vec{r})/\rho^{5/3}$ and $C(\vec{r})/C_h(\rho(\vec{r}))$.

It is evident from the definition of ELF in Equation 6 that the scale has been established more or less arbitrarily. This fact is irrelevant in graphical representations as the numerical scale is transformed into a (arbitrary) color scale or is shown in the form of isosurfaces (selected arbitrarily in three-dimensional representations). No information is lost as electron pairs and the chemical bond are first and foremost examined qualitatively. It must be mentioned that qualitative statements can also be described mathematically (for example the catastrophe theory of R. Thom,[18] which was used by Bader and co-workers[12] in analyzing the density). We now want to comment on this aspect in connection with ELF.[19] As we have decided to focus on the

characterization of pair regions, those regions where ELF exhibits maxima are of special interest. Mathematically, it is known that the positions of maxima may be sought by examining the first derivative of a function. For ELF they are fulfilled by the first derivatives of C/C_h; thus, for this property the second scaling rule is irrelevant. ELF can have several maxima. The positions of these maxima are denoted as *attractors*. The next step is the division of space by considering the path of steepest ascent (the gradient of ELF) from every point in space. If an attractor is found along this path, the point is assigned to it. All points in space from which this attractor is reached form its *domain* (Wirkungsbereich, WB). Thus, we obtain a more precise definition of the "pair regions".

Another way to analyze ELF is to examine the spatial region (the *f-localization domain*) in which $ELF \geq f$ is valid, where f is a constant.[19, 20] For larger values of f there is only one attractor in each of the f-localization domains. At a certain (smaller) f-value different f-localization domains come into contact at a single point (an ELF saddle point; again only the relation C/C_h is important because we are dealing with the first derivative). Smaller values of ELF lead to a merging of these localization domains: here the f-localization domain contains more than one attractor. The f-interval, where only one attractor in the f-localization domains exists (the difference of the ELF values at the maximum and the saddle point), is characteristic of the bond. The separation between the core and valence regions is more sharply defined than the separation observed within the valence shell. In particular, the separation of the regions of double-bond pairs is weak.[21]

Of course, quantitative statements can also be obtained with ELF. Quantifications of charge, volume, etc. can be determined. A total electron number can be obtained upon integration of the electron density in a certain domain (see Section 4.2). ELF yields electron numbers that are usually in agreement with chemical intuition, for example two for a region assigned to a pair of electrons. On the other hand, special electron numbers appear due to the above-mentioned overlap effects, such as $\approx 3/2$ for the C–C bond in benzene or ≈ 8 for the valence shell of the Ne atom.[22] Remarkably in ionic solids, ELF predicts electron numbers that correspond to those derived from formal charges.[23]

The precision of the determination of such electron numbers is interesting. According to the Heisenberg uncertainty principle, the above-mentioned numbers can only be considered as mean values. But it is possible to get average deviations. These deviations are relatively small when dealing with atomic cores, whereas for valence electrons they are larger.[21] More sophisticated calculations show that the partition obtained by ELF resembles the one yielding the smallest uncertainty.[24]

Although ELF is currently only obtainable from calculations, it is, in principle, possible to derive ELF from experimental data. Certainly, the evaluation of the sum of the squares of the wave function (and the pair density) according to the postulates of quantum mechanics is a possibility; but this is more difficult to realize. Therefore, we want to show how ELF can be determined from the electron density alone, and in the following we present a definition of ELF equivalent to that given before.[25]

A computational method that is successfully applicable for molecules as well as for solids is based on the (exact) density

functional theory defined by Kohn and Sham.[26] Therein the ground state energy is exclusively determined from the electron density. The terms in the energy expression can either be easily calculated from the density (the classical interaction of the charge distribution), or sufficiently approximated (the exchange and correlation energy). However, the construction of the kinetic energy can cause difficulties if the Pauli principle is neglected. In the density functional theory defined by Kohn and Sham, the kinetic energy of a hypothetical system T_s with identical density but no interaction between the particles is calculated instead of the kinetic energy from Equation (1). This leads to a simplification and the ground state function is (usually) a Slater determinant so that the orbitals in Equations (1) and (4) are not singly or doubly occupied (i.e.: $n_i = 0$, 1, or 2).

If the Pauli principle is ignored, it has been shown[27] that all electrons will occupy the orbital of lowest energy, which is defined by $\varphi_i = \sqrt{\rho(\vec{r})/N}$ (N = electron number). Therefore it is possible to evaluate the increase in kinetic energy that occurs on consideration of the Pauli principle [Eq. (9)].

$$\Delta T = \int \left[\frac{1}{2} \sum_i |\nabla \varphi_i|^2 - \sum_i |\nabla \sqrt{\rho(\vec{r})/N}|^2 \right] d^3r \qquad (9)$$

Upon applying the same scalings used for ELF (electron gas, interval $(0,1)$), the integrand yields a local value that corresponds exactly to the expression of the ELF formula [Eq. (6) with Eqs. (3)–(5)]. These orbitals, which yield the exact density, are not easily obtained from the electron density, but this is possible with several algorithms and programs (see, for example, ref. [28]).

To investigate the role of approximations in ELF calculations, densities (and no other information) determined by exact calculations on small atoms were used. ELF values were obtained that fortunately do not differ significantly from the Hartree–Fock (HF) and density functional calculations that are routinely carried out.[29] Even rather simple methods, such as the extended Hückel method (EHMO), reveal the characteristic features of ELF.[16, 30, 31] There are other interpretations of ELF but all of them are based on the Pauli principle.

2. Fundamental Studies of the Chemical Bond

In the first publications on the practical applications of ELF, the ability of the function to generate easily understood pictures of the chemical bond for many different chemical systems was demonstrated.[32] Subsequently, many more chemical systems have been examined, all of them substantiating this result: ELF yields very meaningful, easily understandable, and visually informative patterns of the chemical bond. In this section we want to analyse some typical chemical bonding forms with ELF. We will demonstrate how ELF portrays these forms, and the similarities and differences to other existing methods will be highlighted. It has been shown that pictures obtained with ELF by using different theoretical calculation methods are qualitatively comparable (see Section 1). Here, we present results obtained by using the relatively simple extended Hückel approximation[33] and the more sophisticated ab initio linear-muffin-tin orbital method (LMTO).[36]

A single krypton atom serves as an example to explain the shell structure of atoms in the ELF pattern. Figure 1a shows
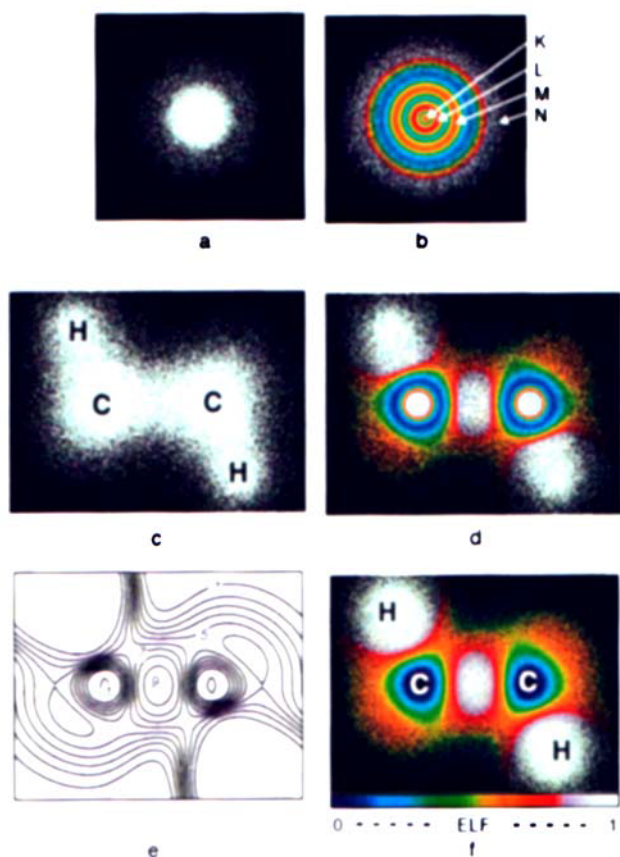
Figure 1. Distribution of electron density a) in a section through a krypton atom, c) in a section through an ethane molecule and coloring with ELF b) and d), respectively, based on HF calculations. The color scale for all such ELF representations corresponds to that given in Figure 1 f. e) and f) Representation of ELF for the EHMO valence electron calculation of ethane with contour lines and the corresponding ELF representation with colored valence electron density, respectively.

using pseudopotentials. In such calculations, the problem is restricted to the quantum mechanical treatment of valence electrons, while interactions with the core electron density are substituted by effective potentials. Figure 1 e depicts ELF in terms of a contour line diagram.

In the series ethane, ethene, and ethyne (Figure 2) differences between covalent single, double, and triple bonds are clearly seen.[40] This is valid for both representations: the two-dimensional (2D) cross sections in Figures 2 a, c, e, and g as well as the three-dimensional (3D) isosurfaces in Figures 2 b, d, f, and h. It
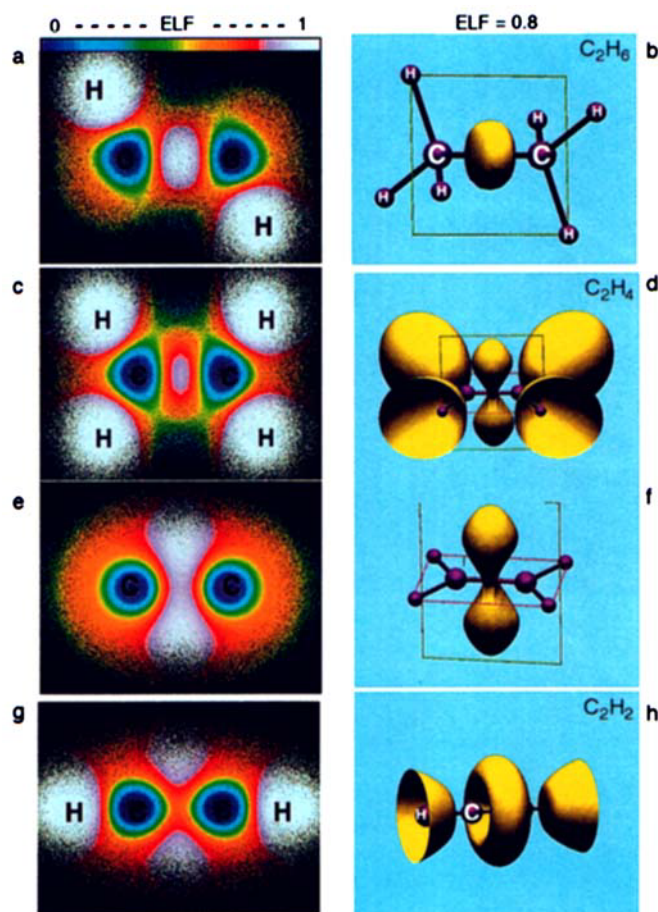

Figure 2. Left: 2D cross sections (EHMO calculations) through the molecules a) ethane, c) and e) ethene, and g) ethyne. Right: 3D representations of ELF isosurfaces with ELF = 0.8, b) ethane, d) and f) ethene, and h) ethyne. The planes around the hydrogen atoms are either not shown or only cut.

only the electron density for the free atom, whereas in Figure 1 b this point pattern is colored according to the ELF values. Thus, in such two-dimensional graphical representations the electron density (as a density of points) and the ELF values (coded in a color scale in analogy to a geographical map) are depicted simultaneously. High ELF values (approximately 0.8 to 1.0) are colored white; the series descends through brown and yellow to green for middle ELF values (ca. 0.5). The lower end of the scale is represented by blue and violet.[39] Of course, it is possible to reproduce ELF in two dimensions by using contour line diagrams. In three-dimensional representations, isosurfaces are shown for each chosen ELF value.

Four separate localization shells with varying degrees of contraction and compactness can be recognized in the krypton atom. In the course of our discussion we will focus on the regions that can be assigned to either atomic cores or to valence electrons. Figures 1 d–f depict the ELF representations for sections through the ethane molecule along the C–C bond. It is known that the electron density is poorly structured (Figure 1 c), whereas all chemical details of the structure can clearly be discerned in the ELF representation: the C atom cores and the C–C as well as the C–H bonding regions. The latter are diffuse and also show the H positions. In the EH valence electron calculation (Figure 1 f), regions of low localization appear instead of the C-atom cores. A similar result is obtained with calculations

should be pointed out here that the number and form of the localization regions are strongly dependent on the choice of the isovalue. An isovalue of ELF = 0.8 has proven to be a useful standard for the classical valence compounds; this corresponds to the white-orange border in the 2D cross sections. In both representations an increasing contraction of the σ-like region along the C–C axis is observed with the increase of bond order. The 3D representation of ethyne gives the impression that only a localization torus is present. HF calculations using a double-zeta basis set and polarization functions[29] show that this is correct in principle. With both methods (EH, HF) the highest electron density is found on the core–core connecting line (Figure 2 g) but the highest ELF values are found outside (Figure

2f). The torus obtained from EH calculations is more distinctive. In conclusion, this result corroborates the formally equivalent descriptions of double bonds previously formulated by Pauling:[41] the banana or bent bonds and the σ-π-bonding model.

In electron-rich compounds, lone pairs of electrons play an important role in structure formation. Their structure-directing influences are summarized by the rules of Nyholm and Gillespie (VSEPR model[1]). These rules have been used successfully for decades and although they are more or less intuitive, only recently have quantifications been attempted.[42]

Figure 3 shows the 3D ELF isosurfaces for PF_3, SF_2, ClF_2^-, and ClF_3. As expected, the geometrical distributions of lone
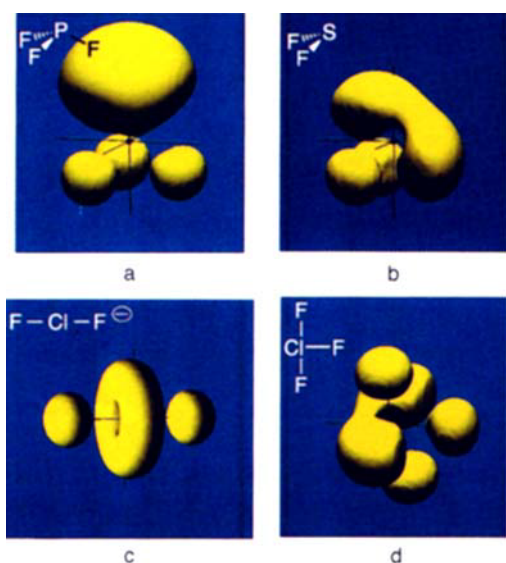

Figure 3. 3D representations of ELF isosurfaces with ELF = 0.8 for molecules differing in the number of lone pairs (based on EHMO calculations): a) PF_3; b) SF_2; c) ClF_2^-; d) ClF_3. The positions of the fluorine ligands (within the yellow ELF regions) can be taken from the given structure formulae. The central atom is located at the origin of the coordinate system shown in each figure.

pairs of electrons and bonding electron pairs and ligands correspond in principle to the VSEPR model: extended regions of lone pairs of electrons and relatively compact, almost spherical localizations around the F ligands. A closer inspection of the latter reveals a division in regions of element–F bonds and lone pairs of electrons at the F center.[16, 32] The contraction of the lone pairs of electrons is very evident in going from the relatively extended region at P in PF_3 to the compact torus at Cl in ClF_2^-.[43] The exceptional *anti*-position of the lone pairs of electrons both in SF_2 and ClF_3 is more distinctive than expected from the VSEPR model.

The topological similarity between ethyne C_2H_2 (Figure 2h) and ClF_2^- (Figure 3c, ref. [44]) is also interesting. These units are clearly distinguished by chemists but they are equivalent with respect to the attractor model (see Section 1). In other words, the attractor may be bonding (C–C bond) as well as nonbonding around the Cl atom. In this sense it is possible to deduce a hierarchical relationship even for these two simple species (ref. [121], see Section 7.2): the topology of the attractors is the same but the chemical structure realized therein is diversely complex.

In addition to the examination of the real electron space, cores, bonds, and lone pairs and their mutual interactions, be-

come visible in simple molecules. In organic chemistry these interactions are understood by using qualitative concepts. Methyl acetate CH_3COOCH_3 serves as an example (Figure 4).[40] The three-dimensional representation of the ground
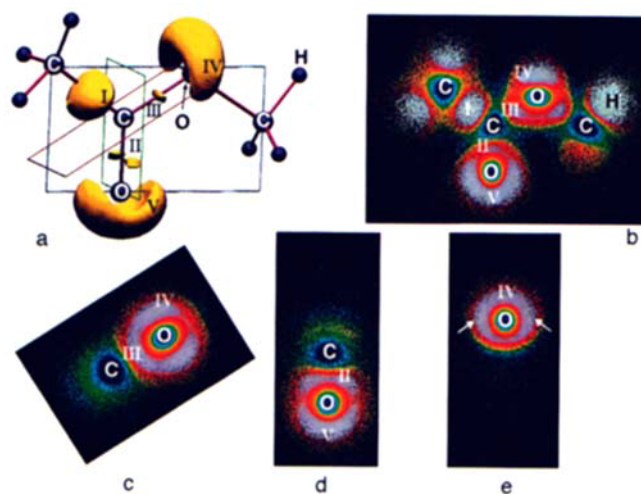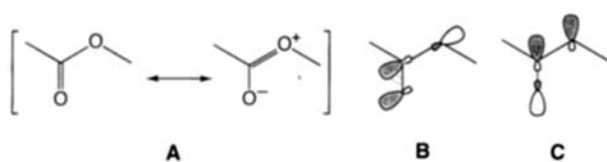

Figure 4. a) 3D representation of the ELF isosurface ELF = 0.85 (EHMO calculations) for methyl acetate. The regions around the hydrogen atoms are not included. For ELF = 0.80 the regions of the lone pairs (IV and V) are no longer separated from the neighboring C–O bonding regions (III and II, respectively). b)–e) 2D cross sections through different planes: b) through the plane drawn in blue in (a); c) through the plane drawn in red in (a); d) through the plane drawn in green in (a); e) through the plane parallel to that drawn in (d), which contains the oxygen atom of the ester.

state conformation contains an ELF isosurface showing extended localization domains for the lone pairs of the carbonyl and the oxygen atom of the ester. In addition there is a relatively extended region that includes the C–C bond (for clarity the C–H bonds were not included in the calculation of ELF). On the other hand, the regions of C–O single and double bonds are comparatively strongly contracted but show the expected distributions with respect to the core–core bond lines. ELF sections were calculated for planes through the molecule (Figures 4b–e). The cut through the C–O ester bond perpendicular to the molecular plane (Figure 4c) shows a broadening in the bond region in agreement with a double-bond contribution as given in Scheme 1 A. Such an ELF analysis is helpful in the assignment of resonance formulae. Furthermore, a n-σ* anomeric effect is expected between the lone pair at the carbonyl oxygen atom and the σ bond to the ester oxygen atom (Scheme 1 B). This should lead to a deformation of the ELF distribution around the oxygen atom of the carbonyl group, as can indeed be seen (Figure 4b, regions II and V merge asymmetrically). However, the n-σ* interaction in the ester bridge (Scheme 1 C) is not supported by ELF, though the difference in the comparable sections through the oxygen atoms is striking (Figure 4b region V and Figure 4e region IV). The ELF distribution at the oxygen atom of the ester has a slight p-characteristic (the local maxima facing each other in region IV of Figure 4e, marked with arrows), which may be interpreted in terms of a reduction of the s part of the lone pairs (Scheme 1 C).

Investigations of carbosilanes proved ELF to be a powerful tool in the comprehension of complicated bonding systems. It was shown for 1,3-disilacyclobutane that there is no (not even

Scheme 1. Bonding features in methyl acetate.

weak) bond between the two Si centers in spite of a relatively short interatomic distance. Therefore an alternative interpretation was necessary: the Si–C bonds appear as bent bonds in the ELF analysis, and they can be interpreted in terms of a bent bond between two building blocks, which differ in size but retain tetrahedral angles at the cores. From this description it follows that the relatively short Si–Si distance is a geometrical consequence of the bent Si–C bond.[45] Analogously, the bond shortening in C_2H_4 compared with that in C_2H_6 was previously explained by Pauling with the assumption of bent bonds.[41]

2.1. Covalent versus Ionic

The division of chemical bonds into homopolar or primarily ionic bonds has proved to be very useful in the language and comprehension of chemistry. Naturally, the ideal covalent bond is simply defined in element–element bonds but, strictly speaking, only when the surroundings of both bonding partners are identical. The ideal ionic bond with a complete charge transfer does not exist. In general, a bonding interaction intermediate to ionic and covalent bonds is observed: a polar bond.[46]

The definition of the range of influence for ELF attractors permits a new formulation of ionicity in which the delimitation and mutual significance of covalent and ionic parts is simplified.[47] First, a qualitative impression is gained upon analyzing the form of the attractors. If they are more spherically distributed around the cores either a more ionic or a van der Waals interaction is present. If the covalency of a bond increases, the migration of the attractor becomes more distinctive between the centers until a totally symmetric topology is achieved in the ideal covalent case. The position of the attractor between the centers can quantitatively be used to define the extent of polarity of a chemical bond.[48] As long as the attractor lies on the line connecting the cores and can be separated from the cores themselves by a trajectory, and the attractor does not circumscribe the core, a situation is reached that is usually described as polar covalency. An ionic formulation is suitable if the attractor is close to the core region of one of the atoms and no longer on the connecting line. One must take into account that no clear separation is possible.

The combination of the division of the electron density according to Bader[12] and ELF in domains (WBs) is a second way for a complete quantitative description of the chemical bond. The actual charges of the atoms can be determined by the partition of the density in ranges of atomic influence. The covalent contribution of the bond is obtained by the number of electrons in the mutually shared electronic range of influence and attractor (partition of ELF). This is illustrated in Section 4.2 with the results of calculations on several intermetallic phases.

2.2. ELF in Simple Crystal Structures

The investigation of structure and chemical bonding is frequently carried out with a small number of ELF plots, where series of structures can visually be compared. In this way the language of ELF can be learned "simply", asking the basic question: "what happens if…?". Figure 5 illustrates ELF for sections through simple structure types with primitive cubic arrangements and their AB variant, the rock salt structure, (Figures 5a–d), as well as the diamond structure and its AB variant, the zinc blende structure (Figures 5e–h). The ELF obtained from LMTO calculations on the isoelectronic series silicon ("SiSi"), AlP, MgS, and NaCl are shown. The corresponding hypothetical modifications are given in quotation marks.
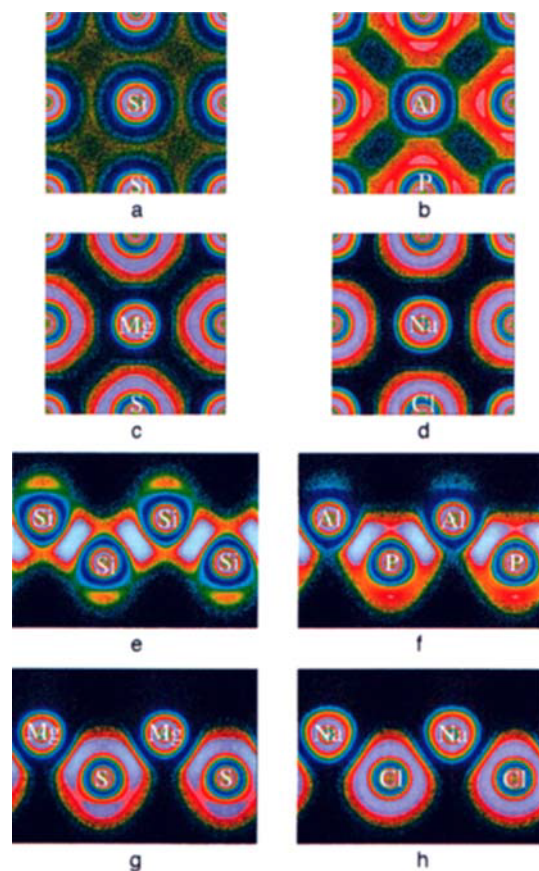

Figure 5. ELF sections (based on LMTO calculations) for the (100) surface of a) a hypothetical primitive cubic structure of silicon, as well as for the rock salt structure for b) AlP, c) MgS, and d) NaCl. The increasing concentration of regions of high ELF values on spherelike shells around the cores is evident. e)–h) Actual and hypothetical modifications of diamond structure: e) silicon, f) AlP with a clearly increased bond polarity, g) MgS with polarized "S^{2-} ions", and h) NaCl with clearly separated but still polarized anions.

"Silicon" in a primitive cubic arrangement would be really lost in a metallic state: the valence electrons are totally delocalized over that region which is not covered by the cores (Figure 5a). A localization of ELF ∼ 0.7 is rather high with respect to the free electron gas (ELF = 0.5). For the corresponding "AlP" phase, ELF provides an almost perfect example of a polar bond: it increases in a wedge-shaped fashion from the Al core to the phosphorus atom, where it merges with five other

equivalent localization domains (Figure 5b). It should be mentioned that the individual localization regions can be separated by trajectories of minimal function values (orthogonal trajectories). This can be used for the division into domains (WBs) and for subsequent quantitative evaluations (see Section 4.2).

For MgS, ELF indicates a more ionic structure. The soft S^{2-} ions are polarized, resulting in an octahedral distortion of the spherical symmetry (Figure 5c). In NaCl, a region of high localization with nearly spherical symmetry is found around the anion (Figure 5d). If a corresponding division of ELF is made, no attractors can be found between the Na and Cl atom pairs. Rather an alignment of the attractors is found as expected on the basis of the VSEPR or ligand field theory.[49] The six attractors around the chloride ion are directed precisely between the Na neighbors. Whether the disappearance of the attractors from the line connecting interatomic centers is suitable for a sharp separation of polar-covalent and ionic bonds must be further investigated as very polar π or δ interactions cause similar effects.

From the general evolution of the localization in the former case it can be concluded that an increase in the localization in the vicinity of certain attractors leads simultaneously to its decrease in the interstitial regions. With respect to the free electron gas, whose density is totally uniform and revealed by the green coloring in ELF (see Section 1), a more or less distinctive localization of electrons takes place in every structure. In the primitive cubic packing of identical atoms (Figure 5a), the proximity to the electron gas is even more pronounced. For example, Savin showed a dramatic alteration of the localizations with different valence electron numbers in the fcc structure. For calcium (2e per atom) the localization regions are in the octahedral holes, whereas in aluminum (3e per atom) the regions of highest localization are always found between the Al pairs[50] (see Figure 12o). On average, the localization for silicon in the bonding region is even higher but the distribution is distinctively less structured than in the aluminum case.

In compounds exhibiting the diamond structure (Figure 5e–h), localized regions are only present in sections of ELF along the plane diagonal of the unit cell ([110]). In this series the localization maximum is again shifted stepwise along the core–core connecting line towards the more electronegative atom. The position of the ELF maximum can be used to measure the extent of the polarity of the bond. Even for "NaCl", a considerable deviation from the spherical symmetry of the anions is observed (Figure 5h). Examination of the plots reveals that AlP appears to be predominantly covalent, whereas "MgS" and "NaCl" are more ionic, because of an increasing spherical distribution of the localization around the anions. In "NaCl" the appearance of a strongly polarized anion is predominant. In AlP and MgS it is possible to clearly distinguish between the regions of localization of high ELF values. For the more ionic compounds, such distinctions are hardly or often not possible. The immediate impression gained from these ELF representations confirms those gleaned from chemical intuition.

Similar ELF investigations of the diamond structure for the elements carbon, silicon, germanium, and tin also show interesting trends; a reduction of localization in the two-electron–two-center bond, while the localization in the interstitial region in-

creases continuously.[25] The comparison of α- with β-tin clearly verifies that in the latter a much lower localization is present than in the diamond modification.[25]

2.3. Bonds between Metals

One faces the metallic bond as if one is meeting an alien: with suspicion, lack of understanding, and a certain respect. The actual meaning of the term "metallic bond" is complex with many variations and we will examine it in more detail in Section 4. First we consider the smallest metal aggregations, biatomic clusters[16] such as $[Re_2(CO)_{10}]$, $[W_2(CO)_8]^{4-}$, and $[Mo_2Cl_8]^{4-}$. The question is: may bonds between transition metals be resolved as well as those between main group elements?

According to the 18-electron rule $[Re_2(CO)_{10}]$ and $[W_2(CO)_8]^{4-}$ should have one and two metal–metal bonds, respectively. Four metal–metal bonds are expected in $[Mo_2Cl_8]^{4-}$. Figures 6a–c present the structures of these clusters with the accompanying 3D ELF isosurfaces as calculated with the EH method. As expected, for $[Re_2(CO)_{10}]$ a rotationally symmetric localization is found between the metal centers that is relatively small compared to the localization regions around the CO ligands (Figure 6a). This holds also for the two other clusters: the corresponding localization regions are very compact in spite of the contribution of 4d and 5d states. This is generally observed
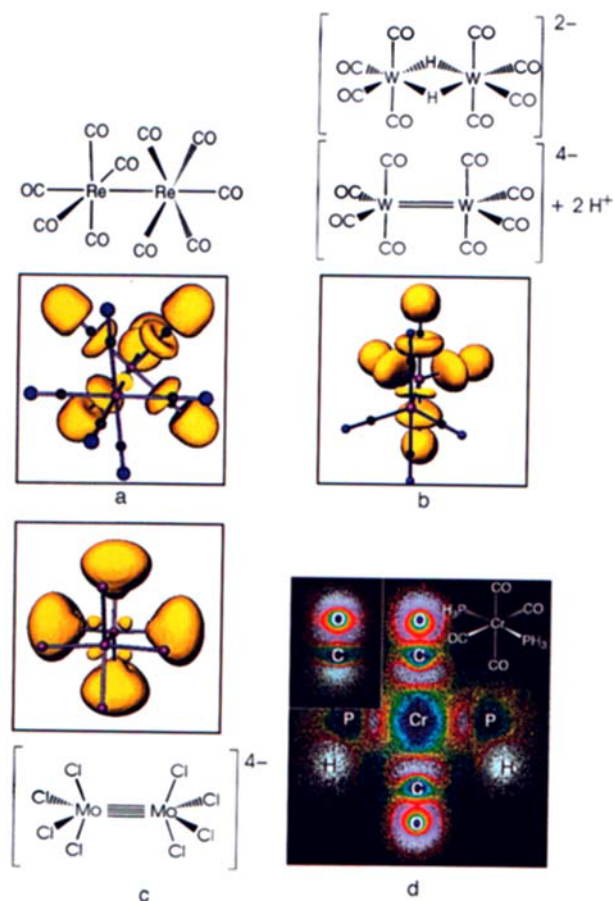

Figure 6. 3D representation of the isosurface ELF = 0.80 for molecules with a) metal–metal single, b) metal–metal double, and c) metal–metal quadruple bonds (EHMO calculations). d) 2D section through a plane in $[Cr(CO)_4(PH_3)_2]$ and 2D cross section through a free carbon monoxide molecule (insert).

in systems containing transition metals. As a rule, regions of ELF with high contributions of d states are rather small both with respect to the ELF values and the volume.

In the case of $H_2[W_2(CO)_8]^{2-}$, a π-like distribution between the metal centers is indeed observed in the deprotonated form $[W_2(CO)_8]^{4-}$ (Figure 6b). Of course, in this case the double bond is aligned in this special way only because the arrangement of the CO ligands breaks the degeneracy of the two possible π states. The two possible formulations $2H^+ + [(CO)_4-W=W(CO)_4]^{4-}$ and $[(CO)_4W(\mu_2-H)_2W(CO)_4]^{2-}$ again show the hierarchical relationship, which is evident at the ELF attractor: the attractor is able to accommodate electrons as well as atoms and ions or multicentered groups without changing the topology of the total system.

For $[Mo_2Cl_8]^{4-}$, ELF shows four localization regions around the line connecting the M centers. This can be understood in terms of four bent bonds (Figure 6c). Taking into account that the point group D_{4h} allows only a twofold degeneracy, a principal difficulty arises, which also appears in the MO description of methane. The problem is that we do not have a "natural sense" for degeneracy caused by symmetry. At first the chemistry student is surprised at the strange partitioning of spherical symmetry into one s, three p, five d, seven f etc. representations but this is quickly accepted. It is a matter of debate whether $[Mo_2Cl_8]^{4-}$ actually "believes" its electronic structure may be reduced into irreducible representations. It must be emphasized that ELF always provides a picture that corresponds to the full symmetry of the respective group. This property is reminiscent of the symmetry-adapted hybrids of the VB theory, but it must be stressed that in contrast, ELF is always unambiguous.

Finally the ELF at the ligands is also worth mentioning. A comparison of the CO groups in Figures 6a,b reveals an extended region that surrounds the polar triple bond and the lone pair around oxygen. In $(H^+)_2[W_2(CO)_8]^{4-}$ it is smaller and more round, whereas the region between W and C atoms is more extended. Figure 6d shows the sections of ELF through an isolated CO molecule and in the octahedral complex $[Cr(CO)_4(PH_3)_2]$. Clear displacements of the localization regions are found when the free and bound CO molecules are compared. Here, the differences between a strong CO–Cr and a normal donor P–Cr bond are evident. Similar results were obtained recently by Kaupp in the analysis of two-center carbonyl clusters with terminal and bridging CO ligands.[51]

To substantiate this result we carried out EH calculations on the following series: free CO, $[CO-Cr(CO)_5]$, and $[CO-Cr(CO)(PH_3)_4]$ (Figure 7[52]). A distinct bonding effect between chromium and the CO ligand is expected and can clearly be seen by comparing the left part and the center of Figure 7. In $[CO-Cr(CO)_5]$ the attractor lies on the Cr–C bond axis (center), whereas in $[CO-Cr(CO)(PH_3)_4]$ this axis is surrounded by a torus (right), which indicates the presence of π-bonding contributions. In the first case the metal–ligand backbonding is relatively weak because the Cr center has to distribute its electrons evenly onto six ligands; thus, the σ character is dominant.

From these examples it is evident that in organic molecules (Section 2, Figure 4) as well as in complexes, weak effects such as changes in the behavior of backbonding become directly visible with ELF.
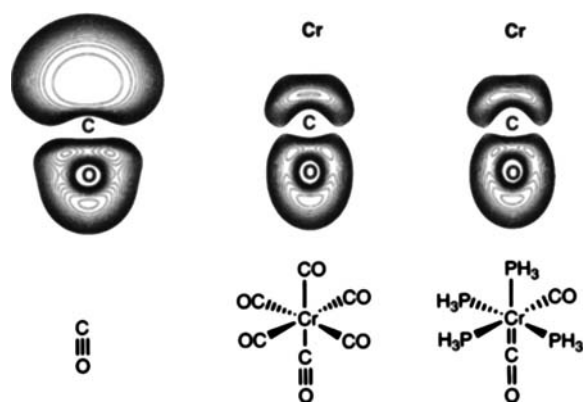

Figure 7. Contour line representations of the ELF (EHMO calculations) through a free CO molecule (left), CO complexed in $[Cr(CO)_6]$ (center), and in cis-$[Cr(CO)_2(PH_3)_4]$ (right) with the corresponding valence line formulae.

2.4. Clusters, Multicenter Bonds, and the Principle of Duality

The boranes, carboranes, and naked clusters (especially those of the heavier elements of group 14) form deltahedral clusters that may be understood with the aid of Wade's rules.[53] Here, terminal lone pairs and terminal bonds on the cluster are separated from the framework states as one- or two-center states. The framework bonds can be formally described as local three-center interactions in the sense of closed three-center bonds.[54] However, this leads to problems because, as a rule, there are more triangles than occupied framework states in closo deltahedrons. Here, a kind of inverse problem to that discussed in both the examination of multiple bonds (Section 2.3) and benzene (Section 1) arises. This forces the formulation of mesomeric structures, that is formulations coinciding with the phenomenon of delocalization (at least in the conventional sense).

What pictures are provided by ELF with regard to framework electrons and framework–ligand interactions, and how do ELF distributions change with respect to the number of framework electrons?

The first ELF examination of boron clusters revealed a pronounced duality between the polyhedral framework and the localization regions. The latter form the dual tetrahedron for the tetrahedral B_4H_4 framework, a cube for the octahedral $B_6H_6^{2-}$ ion, and a pentagonal dodecahedron for the icosahedral $B_{12}H_{12}^{2-}$ ion.[30] Recently theoretical studies based on experimental investigations were carried out on B_9X_9 (X = Cl, Br, I), the findings from which add further support to this interpretation.[55]

Figure 8c shows ELF for a $B_6H_6^{2-}$ cluster.[16] The localization regions above the planes are clearly seen and simultaneously a noticeable localization appears above the edges. A systematic study of ELF versus the number of framework electrons n_G reveals localization regions that are either spherical ($n_G = 2$, Figure 8a), concentrated above planes ($n_G = 8$, Figure 8b), distributed above planes and edges ($n_G = 20$, Figure 8d, Wade's framework electron number), or only above the edges ($n_G = 20$, Figure 8d). For main group element clusters, twenty electrons corresponds to a strongly antibonding situation. If d states are present at the metal centers up to twelve orbitals must be occupied before antibonding states are reached. The $[Mo_6Cl_8]^{4+}$ group found first in $MoCl_2$[62] has 24 framework electrons and

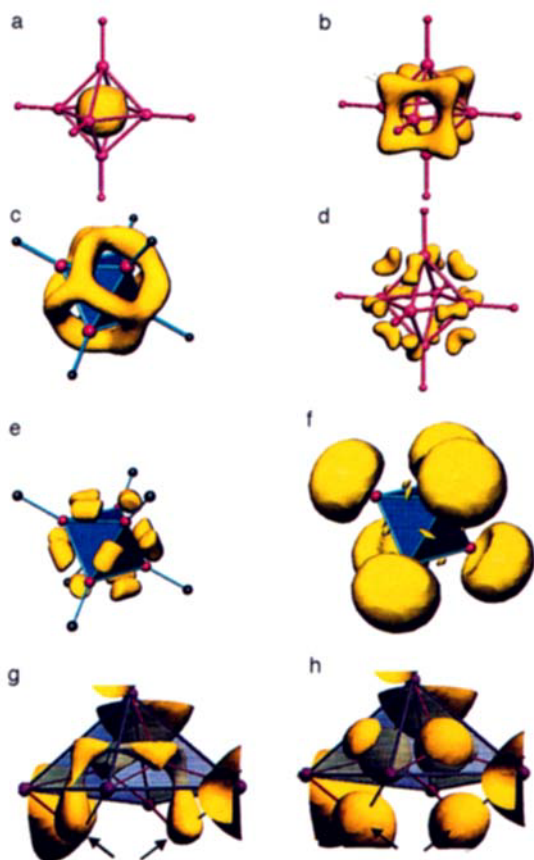*Angew. Chem. Int. Ed. Engl.* **1997**, *36*, 1808–1832

1817

Figure 8. 3D representations of the ELF = 0.80 isosurface for different cluster molecules (EHMO calculations). a)–d) Octahedral clusters with different numbers of framework electrons n_G, each calculated with the parameters used for the calculation of $B_6H_6^{2-}$. For details see text. e) $[Sn_6H_6]^{4+}$ as a model for $[Sn_6(Cr(CO)_5)_6]^{2-}$. f) The corresponding hypothetical $[Sn_6]^{2-}$ ion without transition metals. g) and h) ELF isosurfaces of the square-pyramidal clusters $[Zr_5Cl_{12}(PMe_3)_5]^{4-}$ and $[Zr_5Cl_{12}(PMe_3)_5H_4]$, respectively, together with the structure of the Zr_5 cluster unit. The Cl and PMe_3 ligands are omitted for clarity. The arrows mark the positions of the bridging hydrogen atoms. In addition to the spherical localization regions of the four hydrogen atoms, h) shows two smaller regions that are found in the unoccupied triangular planes. The ELF isosurfaces of the isoelectronic and formally fourfold deprotonated cluster in g) are very similar: four almost equal regions above the triangular planes and two distinctive ones above the open plane of the cluster. See text for details.

is representative of the latter situation. For such systems variable numbers of framework electrons ranging from 19 to 24 have been verified experimentally.[56]

The duality relationship was already pointed out in investigations of metal carbonyl clusters[51] and for clusters in intermetallic phases.[57] Again, this is only valid for certain numbers of framework electrons, for example for main group element clusters with electron numbers close to those predicted by Wade's rules.

There are typical examples of octahedral clusters with different electron counts (Figures 8 a – d) that sometimes contain condensed rather than isolated polyhedra. The ELF distribution with two framework electrons is shown in Figure 8 a. The octahedral Li_6C group is an example of such a two-electron system, for which a totally symmetric lithium-centered framework state has been calculated.[58] To our knowledge, the eight-electron case (Figure 8 b) has never been observed. Here, the duality between the framework structure and ELF is most evident. Wade's electron number for the octahedron is achieved with 14 electrons,

whereas the 15e and 16e systems are realized in the well known clusters $[Nb_6X_{12}]^{3+}$ and $[Nb_6X_{12}]^{2+}$, respectively. Here, almost equally pronounced localization regions above planes and edges of the polyhedron are found as well, but with a slight accentuation above the planes. Clusters with 19 to 24 framework electrons like Nb_6I_{11}, HNb_6I_{11},[59, 60] the Chevrel phases,[61] and $[Mo_6X_8]^{4+}$ are examples of 20e systems with very distinctive concentrations of regions of high localization above the edges of the polyhedra (Figure 8 d). The shape of the localization regions in $B_6H_6^{2-}$ as well as in $[Zr_6Cl_{18}]^{8-}$ and $[Nb_6Cl_{18}]^{4-}$ (14 and 16 framework electrons, respectively) is almost identical. With regard to the framework atoms, the localization regions are located outside of the B_6 cluster, but inside of the clusters in the other two metal polyhedra.[52, 66] Two possible reasons for this are: first, the different size of the polyhedra and the relation of orbital expansion to edge length, and second, the different interactions and repulsions between ligands and framework electrons.

Several examples of clusters with different numbers of valence electrons exist. For instance, $[AuPR_3]_4^{2+}$ [63, 64] and Li_4^{2+} contain two framework electrons, B_4Cl_4 and C_4R_4 eight, and Si_4^{4-} and P_4 twelve. A corresponding spherical distribution is found in ELF. Four localization regions above the planes and six above the edges[16] may be seen in ELF and can be interpreted in terms of bent bonds over the planes.[45, 67, 68] As in the dinuclear metal complexes mentioned previously (Section 2.3), the mutual distribution of ligands and localization regions of the framework is also apparent here: if the ligands are electron-rich octet systems, the ligands and localization regions avoid each other. Here, a kind of higher hierarchical level of the ligand field theory is found. The form and the number of the attractors is not only determined by the type of the occupied framework states, but also by the type of the ligands and their distribution. Therefore, it should be possible to transfer effects like the Jahn – Teller distortion and ligand-field induced changes, which are well understood for mononuclear metal complexes, to topologically related larger systems, that is on a higher hierarchical level. This was carried out many years ago on M_6 clusters such as M_6X_8 and M_6X_{12} by Simon.[56] ELF is especially suitable for the observation of such effects in real space.

Figures 8 e and f show the comparison of the clusters $[Sn_6H_6]^{4+}$ and the hitherto unknown naked cluster $[Sn_6]^{2-}$; the former is used as a model for the recently published cluster $[Sn_6(Cr(CO)_5)_6]^{2-}$. It is clearly seen that electrophilic ligands are bound at the cluster vertices (Figure 8 f). Further ligands would approach the localization regions of the framework. If there are ligands at the edges and vertices of the cluster, localization regions are found at the faces. This is validated experimentally. In $H_7Th_6Br_{15}$, seven of the eight planes of the octahedron are occupied statistically by H atoms. Presumably, they can easily tautomerize above the localization regions on the plane centers and would as such be carried along the localization regions by an "overhead cable".[30] Experimental and theoretical examinations carried out on the $B_6H_7^-$ ion verify such behavior.[69, 70] According to quantum mechanical calculations, the two H atoms in $H_2B_9Br_9$ with anti-conformation are distributed over two planes of the B_9 polyhedron.[55]

Protons bound on cluster surfaces often give rise to problems in structure determination as illustrated in the following example. A compound containing octahedral Zr_6 clusters was ini-

tially published as $[Zr_6Cl_{14}(PR_3)_4]$,[71] and subsequently proven to be $[Zr_6Cl_{14}(PR_3)_4H_4]$.[72] In the structure determination of $[Zr_5Cl_{12}(PR_3)_5H_4]$, which features a square-pyramidal Zr_5 framework, the position of the protons were determined crystallographically.[73] Two of the protons are located in opposite triangular planes of the Zr_5 pyramid and two protons bridge the opposite edges of the open square plane (Figures 8g and h). Whereas the positions in the triangular planes are located in or above the center of the Zr_3 triangles for reasons of symmetry, there are more degrees of freedom for possible positions above the edges. The ELF investigation of the fourfold deprotonated cluster $[Zr_5Cl_{12}(PR_3)_5]^{4-}$ (Figure 8g) shows four local maxima in the triangular planes and two very pronounced localization regions caused by a slight asymmetrical distribution of the chlorine and phosphane ligands. Their centers correspond exactly to the crystallographically determined positions of the hydrogen atoms.[52] The localization regions are determined only by the electronic structure of the cluster framework and the remaining ligands, independently from the basis functions of the hydrogen atoms used in the calculation. More about the use of ELF in making predictions of structures is given in Section 6.

3. Zintl Phases: Semiconducting Compounds

In the semiconducting compounds M_aX_b (M = metal, X = semimetal) two fundamental chemical classes are united: metals and insulators. In this "symbiosis", the latter component dominates as is reflected in electron structures that are, nearly without exception, described in terms of localized electronic states. In fact, the majority of compounds in this enormously diverse class obey the $(8 - N)$ rule, that is, only two-electron–two-center bonds and lone pairs of electrons are possible states for the valence electrons. Therefore, the electronic structure may be qualitatively determined directly from the topology. As a rule, the connection of semimetals X to give oligo- and polymeric Zintl anions $(X_m)^{n-}$ as well as the coordination of these Zintl anions, which are surrounded by M^{n+} ions through their lone pairs of electrons, may be easily understood from an electrostatic point of view.

The connection pattern is a structural solution to the average connectivity of the X atoms that results from the average valence electron number at X determined from the $(8 - N)$ rule. Bonds and lone pairs form sp^3, sp^2, or sp hybrid-like arrangements around the X atoms with more or less pronounced deviations from the ideal angles as predicted by the Nyholm–Gillespie rules. If there are different structural solutions for the same stoichiometry and the number of valence electrons, the details of the electron structure and a detailed knowledge of the long-range interactions is of interest. Then, local distributions, diffusiveness or compactness, polarizability, and total expansion of local electron density may be important. Only the latter values can be qualitatively and quantitatively examined in three dimensions with ELF.

3.1. Lone Pairs of Electrons in Zintl Phases

The crystal structures of $Ca_{14}Si_{19}$ ($Ca_3Si_{4.071}$) and Ca_3Si_4 differ significantly despite having almost identical formulae and

being in thermodynamic equilibrium at 1270 K.[74] Therefore, a phase transformation is not present here, but a peritectic transformation of the low-temperature (LT) phase Ca_3Si_4 into the high-temperature (HT) phase $Ca_{14}Si_{19}$.

Both compounds contain the bicyclic Si_9 unit (Figure 9a) that appears in $Ca_{14}Si_{19}$ as a sixfold connected building unit $R_6[Si_9^{14-}]$ and in Ca_3Si_4 as a threefold connected unit $R_3[Si_9^{17-}]$. It seems to be that at low temperatures a higher charge can be accumulated in individual regions than at higher temperatures; the distribution of charges and bonds in space becomes more regular at higher temperatures. The average Ca–Si bond lengths of 3.18 and 3.19 Å in the LT and HT phase, respectively, are hardly distinguishable, which is attributable to the almost equal formal overall charges. Apart from the connectivity of the Si frameworks, the Ca atoms have very similar chemical environments with respect to the lone pair electrons.
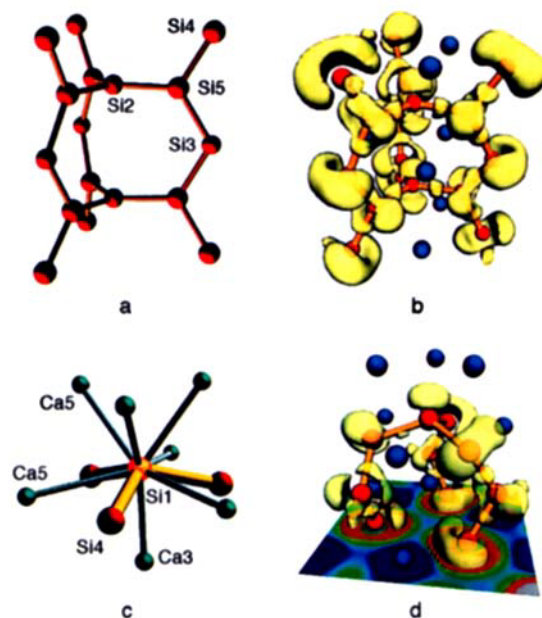

Figure 9. a) Bicyclic unit in $Ca_{14}Si_{19}$ containing the planar Si3-Si4-Si5 chain and planar three-coordinate silicon atoms (Si2, Si5). b) 3D isosurface (ELF = 0.80, based on LMTO calculations) showing very large attractor regions (yellow) for the lone pairs at the two-bonding Si centers and a p-characteristic at the three-bonding Si atoms. c) Bent cap Si1(Si4)$_3$ in Ca_3Si_4. In comparison to that in b), the Ca coordination changes slightly at the Ca5 positions and markedly at Ca3; in this case Ca3 occupies the center of the Si arrangement. d) An enlarged section of the 3D ELF isosurface shown in c) with a similar characteristic distribution of the large lone pair regions. See text for details.

Up to this point, ELF does not significantly enhance our understanding of the structural topology. What is clearly seen with ELF are the enormously extended regions for the lone pair of electrons at the two-bonding Si atoms, which fill the large void that is not occupied by the two bonding neighbors in a horseshoe geometry (Figure 9b). The mutual positions of neighbors and localization regions reveal a relatively good packing of all attractor regions, that is either atomic cores, bonding electrons, or lone pairs (see Figure 9b). In contrast, at the central Si2 atom, which adopts a trigonal-planar coordination, the lone pair clearly has p character. This is also observed at the other three-bonding Si atoms of Si5 type, but the localization regions of the three bonds and the lone pairs are not fully resolved (see Figures 9b and d). Figure 9b clearly shows that

the lone pairs aligned along the Si3-Si5-Si4 chain avoid each other. Furthermore, *the lone pairs do not point directly towards the Ca cations (blue spheres) in the inner region of the fragment. A small change in position of the three-bonding Si1 in Figure 9c is accompanied by an immediate spatial change of the lone pair electron, which now shows a sp³ geometry* (Figure 9d). Therefore it can no longer *take part in the coordination of Ca3. On the other hand, Ca3 polarizes the three* two-bonding Si centers located at the same plane such that the localization regions of their lone pairs deviate from the usual horseshoe form. Overall, it is remarkable that the horseshoe-like lone pairs circumscribe very large spatial regions around the two-bonding Si atoms, perhaps exceeding the effect expected from VSEPR theory. In the 2D cross section of Figure 9d, the cation–polyanion interaction is clearly seen between the yellow localization region and the blue Ca center. The central region of the lone pair is directed towards the Ca atom. We believe that a more extensive spatial examination of this kind with the aid of ELF will lead to a deeper comprehension, because many attractors relevant in structural chemistry become visible in their mutual relations.

The relationship between electron localization regions and cation distribution becomes even more apparent in $Ca_7Mg_{7.25}Si_{14}$,[74–76] because there are two different cations with completely different structural and chemical functions. The compound contains isolated octet Si^{4-} anions and planar Si_{12} groups stacked in an eclipsed manner in the [001] direction (Figure 10a). The regular distribution of large Ca cations around the Si_{12} unit and of the Mg centers at terminal and isolated Si atoms is clearly seen. Despite the large interunit distance of $c = 4.40$ Å, there is a weak interaction that develops between the π states of the Si_{12} group. Such interactions have recently been verified for many polyanionic arrangements of silicon. Band structure calculations on different structures confirm these results.[31] The corresponding EH band structure of $Ca_7Mg_{7.25}Si_{14}$ shows the large dispersion of the π* bands in the c* direction by which the semiconducting characteristic of the bulk of the band structure is overshadowed by a one-dimensional metallic conductivity (Figure 10c, see ref. [31]). This effect is not identifiable in the form of a localized interaction in the ELF, as it is evidently a weak interaction. The quantum mechanical analysis supports a formulation that corresponds only approximately to the Zintl–Klemm formalism, namely $(Ca^{2+})_7$-$(Mg^{2+})_{7.25}[Si^{4-}]_2[Si_{12}^{20.5-}]$. Nevertheless, all ocupied electronic
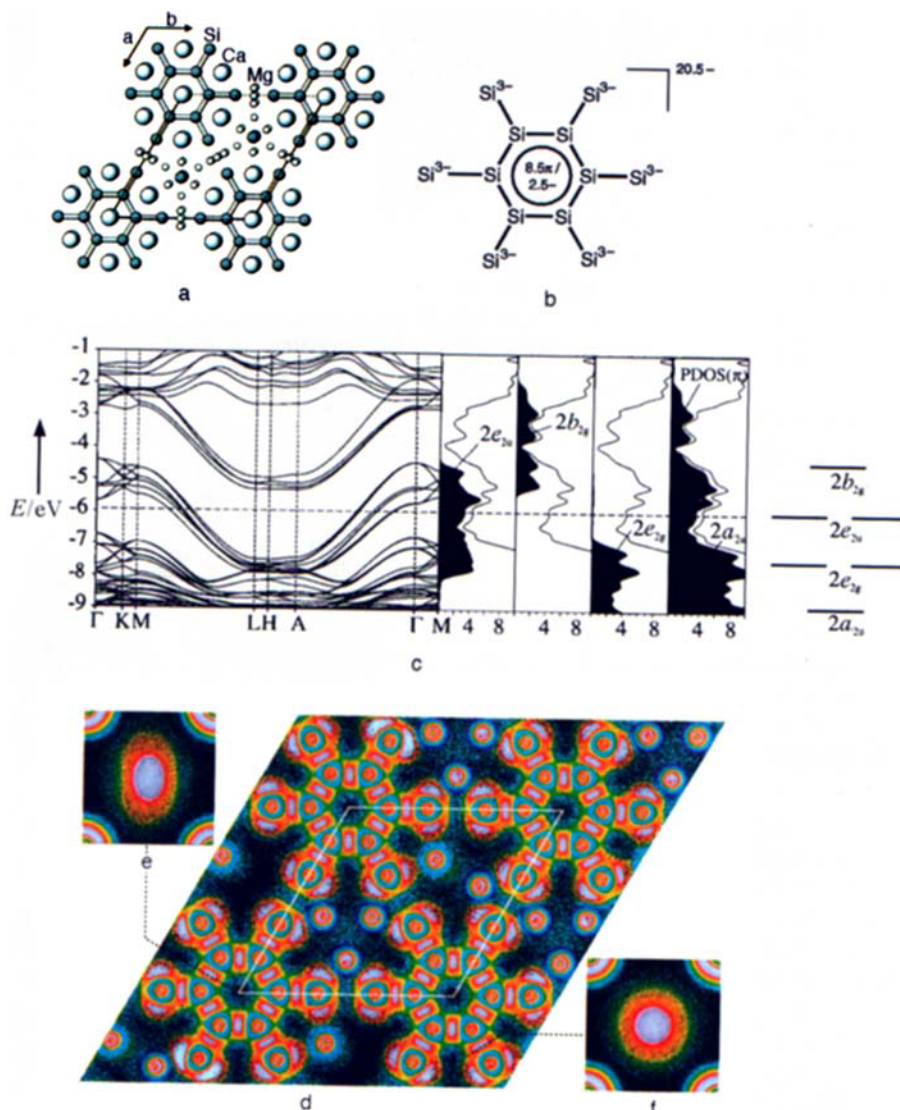

Figure 10. a) Structure of $Ca_7Mg_{7.25}Si_{14}$ containing isolated Si^{4-} anions and planar Si_{12} units. b) Schematic Lewis formula of the planar $Si_{12}^{20.5-}$ Zintl anion. c) EHMO band structure (left), density of states (DOS, center, in states per cell and eV), and MO scheme (pattern) of the π orbitals of $Ca_7Mg_{7.25}Si_{14}$ close to the Fermi level. The band structure reveals bands with large dispersion intersecting the Fermi level. These bands give rise to the metallic nature of $Ca_7Mg_{7.25}Si_{14}$ and are composed of the π* states (e_{2u} symmetry) of the Si_6 ring (left DOS). The comparison between the total DOS (black line) and the DOS of all π states beautifully reveals that despite the metallic conductivity all occupied electronic states are centered on silicon. d) ELF (LMTO) cross section containing Si_{12} rings and several Mg centers. The plot is perpendicular to the c axis of the crystal structure. e) and f) ELF of cross sections of an intraring bond and a terminal bond, respectively, in the Si_{12} ring.

states must be assigned to the silicon anions. Even the conduction band is centered at Si. Therefore, such compounds can be described as metallic Zintl phases. ELF clearly depicts those localization regions that are well understood according to the Zintl–Klemm concept.

An interesting bonding structure can be found in the ELF of the highly charged oligomeric anion $Si_{12}^{20.5-}$. Figure 10d shows the pattern of the Si–Si bonds and the localized lone pairs. Remarkably, the lone pairs clearly interact with the small Mg^{2+} ions, whereas the larger Ca^{2+} ions interact more with the bonding electron pairs and the π system (not shown). This result was also observed in other structures.[31, 74] The relatively complicated band structure (Figure 10c) can thus be brought into a readily interpretable form (Figure 10d) with the aid of ELF.

1820

Angew. Chem. Int. Ed. Engl. 1997, 36, 1808–1832

The 68.5 valence electrons of the $Si_{12}^{20.5-}$ unit occupy the first twelve σ bonds and form the $6 \times 3 = 18$ lone pairs. The remaining 8.5 electron pairs occupy three π-bonding and two π^*-antibonding states. The latter contribute to the conduction band (Figure 10c). Therefore, a π-bonding contribution remains that is unambiguously located in the ring as seen in the bond cross sections shown in Figures 10e and f. The intraring bonds are ecliptically distorted. A distribution of the π-bonding contribution over the whole silicon framework is also conceivable, but such a phenomenon is not observed. The planarity of the polyanions and the absence of significant distortions of the bonding structure in spite of partial occupancy of π^* states is conspicuous here, and has also been observed in numerous other cases of planar Zintl anions. This is due to the relatively high formal and therefore comparatively high effective charges that can only be distributed equally when very delocalized π^* states are generated.[77] Any distortion would lead to an irregular charge distribution, which evidently could not be stabilized by given cation fields.

The structure of the ternary silicide $Ba_2Mg_3Si_4$ contains Si_2 pairs and Si_6 chains.[31] The latter are in the *cis–trans* conformation and planar. The all-*trans* chain is well known for the compounds MSi (M = Ca, Si, Ba), which crystallize in the chromium boride structure type.[78–80] In $Ba_2Mg_3Si_4$ it is conceivable that the *cis* conformation is only present when Mg centers are coordinated to one of the Si centers. The Mg atoms are always in the *exo*- and the large Ba atoms in the *endo*-position to the chain (Figure 11 top). The center of the *trans* connection (of the chain) is always surrounded by four large metal atoms, whereas the highly charged terminal Si centers are always stabilized by four Mg atoms (in both cases only two of these atoms are seen in the figure). This coordination pattern is also found at the Si_2 pair (Figure 11 top). Furthermore, an eclip-
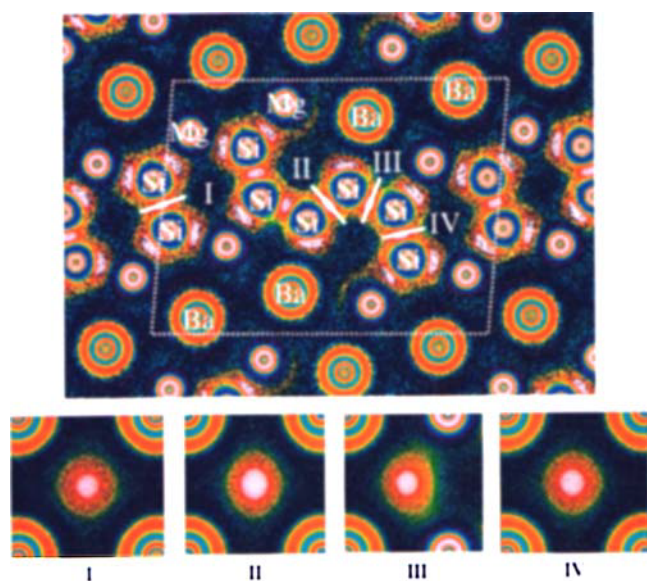

Figure 11. Top: ELF plot (LMTO) of the (010) plane in the new Zintl phase $Ba_2Mg_3Si_4$ [31] that contains Si_2 pairs and Si_6 chains. As in Figure 10, the direct relationship between the Mg centers and the lone pair electrons is demonstrated, whereas the coordination of the Ba cations at the Zintl anions is less pronounced. According to the determined stoichiometry one of the Si_n Zintl anions must contain π contributions. Bottom: The ELF cross sections of the bonds labeled above clearly show that only the six-membered chain contains π contributions. These contributions are very distinctive in the central bond II, weaker in III, and almost absent in IV.

tic packing of Zintl anions along the c axis of the unit cell is present here. Even in this case it is not possible to formulate a completely saturated system with respect to charge balance: $(Ba^{2+})_4(Mg^{2+})_6(Si_2^{6-})(Si_6^{14-})$ and $(Ba^{2+})_4(Mg^{2+})_6(Si_2^{4-})-(Si_6^{16-})$ represent possible formulations of $Ba_2Mg_3Si_4$. In the former case, the six-membered chain is unsaturated (e.g. $[Si-Si=Si=Si-Si=Si]^{14-}$ with 36 valence electrons), in the latter a $[Si=Si]^{4-}$ pair is proposed. Now we want to address the following questions with the aid of ELF:

1. Are there double bonds in Zintl phases and if so, where?
2. What dictates the conformation of the Si_6 chain?
3. Why is there a conspicuous accumulation of Mg centers at the terminal Si atoms?

To answer the first question ELF for a plane perpendicular to the c axis of the structure was analyzed (Figure 11 top). The small representations in the lower part of the figure are sections through Si–Si bonds that are correspondingly indicated in the picture above. There is a rotationally symmetric Si–Si bond in the Si_2 unit that is centered with respect to the interatomic vector (Figure 11, I). It clearly features the characteristics of a σ bond. On the other hand, the central bond in the chain shows an elliptical form and is more extended (Figure 11, II). The Ba atoms come closer to the extended bond, which leads to an enhanced coordination of the π bond. The next bond is markedly distorted towards the Mg centers and shows an elliptical shape in the central, relatively compact region (Figure 11, III). Finally, the bond to the terminal Si atom is almost rotationally symmetric and reveals hardly any π character (Figure 11, IV). This ELF analysis suggests the simplified formulation $[Si-Si \mathrel{\ooalign{\hss}} Si \mathrel{\ooalign{\hss}} Si \mathrel{\ooalign{\hss}} Si-Si]^{14-}$ for the Si_6^{14-} ion. A more detailed analysis of the underlying band structure calculations confirms this formulation. Thus, $Ba_2Mg_3Si_4$ may be formulated $(Ba^{2+})_4(Mg^{2+})_6(Si_2^{6-})(Si_6^{14-})$.[31]

The second question can be answered in light of the geometrical arrangement of cations and lone pairs. Upon comparing the position of the Ba_2Mg_2 groups around bond III with the alignment of the participating Si centers, it is clearly seen that both lone pairs are oriented towards the Mg centers and away from the Ba centers. Therefore, a local *cis* conformation results. In the bonds exclusively coordinated by Ba cations (I, II, and IV), the lone pairs are in the *trans* position, which allows a symmetrical interaction with the cations.

Figure 11 shows that most of the lone pair electrons are oriented towards the Mg centers. It is thus the Mg and not the Ba centers that play the dominating role in dictating the coordination geometry. Therefore it is clear that assuming an equal proportion of cations to anions, the Mg^{2+} ions are able to stabilize higher charges in Zintl anions. This can be predominantly attributed to the higher Coulomb effect. It was previously shown that this structure-directing effect of the Mg cations can be used for controlling the variety of Zintl anions in the solid state.[31, 74, 81]

Finally the spherically symmetric ELF distribution around all metal centers, where only a shell-like structure is visible, should be mentioned, that is, the metal centers act almost as perfect cations. This will be further quantified in Section 4.2. The effective charges of the metal centers are smaller than $q = +2$; however, this is not important as they only stabilize the electronic states of the anions.

Table 1. Classes of chemical compounds, typical building groups, and chemical interactions.

No.	Class of compound	Basic units	Type of interaction
I	van der Waals packings metal packings	atoms, molecules	van der Waals metallic
II	alloys	atoms, clusters, simple structures	covalent and delocalized
III	intermetallic phases	polyhedra, nets, partly complex structures	covalent, ionic, and delocalized
IV	Zintl phases, semiconductors	isolated, oligomeric, and polymeric ions	covalent, ionic
V	insulators	ions, valence polymers	covalent, ionic
VI	coordination compounds	molecules, complexes, and clusters	covalent, ionic
VII	H-bridging systems	polar molecules, valence polymers	covalent, ionic
VIII	composite	combinations of classes I–VI	

4. Intermetallic Compounds

In the past twenty years a great number of novel solid-state inorganic compounds have been synthesized, leading to a deeper understanding of structure–property relationships; thus, we are now able to face intermetallic compounds with new ideas and concepts. The evident conflict between more or less uniform structures of many metallic elements and their often quite complex compounds highlights complicated aspects of the chemical bond, which, however, are gradually being unraveled thanks to the development of theoretical methods. A significant difficulty in transferring classical valence concepts to compounds of classes II and III (Table 1) is their unique structural chemistry and topological form. Obvious relations exist only to boranes and clusters. The definition of intermetallic compounds as a unified family is not so simple; an encompassing theory is not at hand, especially considering the smooth transition to the semiconductors on the one hand and to the alloys on the other, the diverse expressions of the chemical bond, and the extraordinarily rich and varied structural chemistry. Older classifications such as that of B. Pearson (molar volumina, portion of the total energy in the band structure, framework or hybrid-framework structures, ref. [82]) are generally useful but definitely limited with regard to a deeper understanding of the chemical bond. Even the successful division into structure maps does not lead to true understanding.[83]

Also in this context, investigations with ELF led to completely new qualitative but also quantitative insights. We will show in the following sections how the chemical bond in intermetallic phases may be analyzed with ELF. To this end we studied two principal classes of compounds: Type A) those with more homopolar networks and type B) those with cluster-building units.

4.1. ELF in Intermetallic Phases

Figure 12 shows ELF calculations on a series of substances that reveals a transition from the semiconducting compounds to intermetallic phases and to metals in the following order: α-Si, $CaAl_2Si_2$, $SrAl_2$, $BaAl_4$, $CaAl_2$, and α-Al.[84] We assign these phases to type A. The general change in the ELF shows a development of strongly structured, contracted localization regions to distributions revealing not only distinctive structuring but considerably smaller differences between the extrema. The very

high localizations (white regions) decrease proportionally and vary strongly in form and extension. Simultaneously, a change from clearly defined two-center localizations (α-Si, $CaAl_2$, $SrAl_2$) to the coexistence ($BaAl_4$) of two-center (Figure 12i, broad white spots) and multicenter bonds (Figure 12i, small white spots) as well as antibonding interactions (Figure 12j) occurs. The differences in bond lengths in $BaAl_4$, however, are not so dramatic and sometimes counterintuitive: the shortest distance is found for the five-center–six-electron bond (272.5 pm), whereas the two-electron–two-center bond is slightly longer (278.4 pm). An Al–Al distance of 305 pm is indicative of antibonding interactions (Figure 12j) and is quite close to the Al–Al distance in α-Al (286.3 pm). A discussion about bond lengths and bond strengths inevitably fails here.[85] It should be noted that even in $SrAl_2$ and $BaAl_4$ some localization regions show rather high ELF values and therefore yield corresponding integrated electron numbers (see Section 4.2).

The Laves phase $CaAl_2$ and α-Al belong to the class of substances clearly classified as metals; however, distinct localization regions are also present that may be understood in terms of covalent pair interactions even in the case of α-Al. The conspicuously complex structural chemistry of Al compounds, including quasicrystals, is expressed in the highly symmetric cubic closed packing of the metal. A similar case is found in $CaAl_2$, but only for the Al–Al interactions; the Ca–Al contacts are more ionic (Figure 12l, m). There are no Ca–Ca bonding contributions in spite of the diamond-like Ca substructure. Furthermore, all cases show a relatively spherically symmetric distribution of core and very weak valence localization (blue colored) around the large Ca, Sr, and Ba metal atoms, which indicates ionic character. This has been confirmed by quantitative analyses (see Section 4.2).

4.2. Quantitative Investigations

In structural chemistry, geometrical parameters as well as those deduced from topology and composition such as coordination numbers, bond strength, and formal charges have been used for a long time to classify compounds. With skillfully chosen division procedures, model systems are obtained that are sometimes amazingly resilient, but with well-defined limits. More precise statements about, for example, effective or partial charges, or valence electron distributions require other defini-
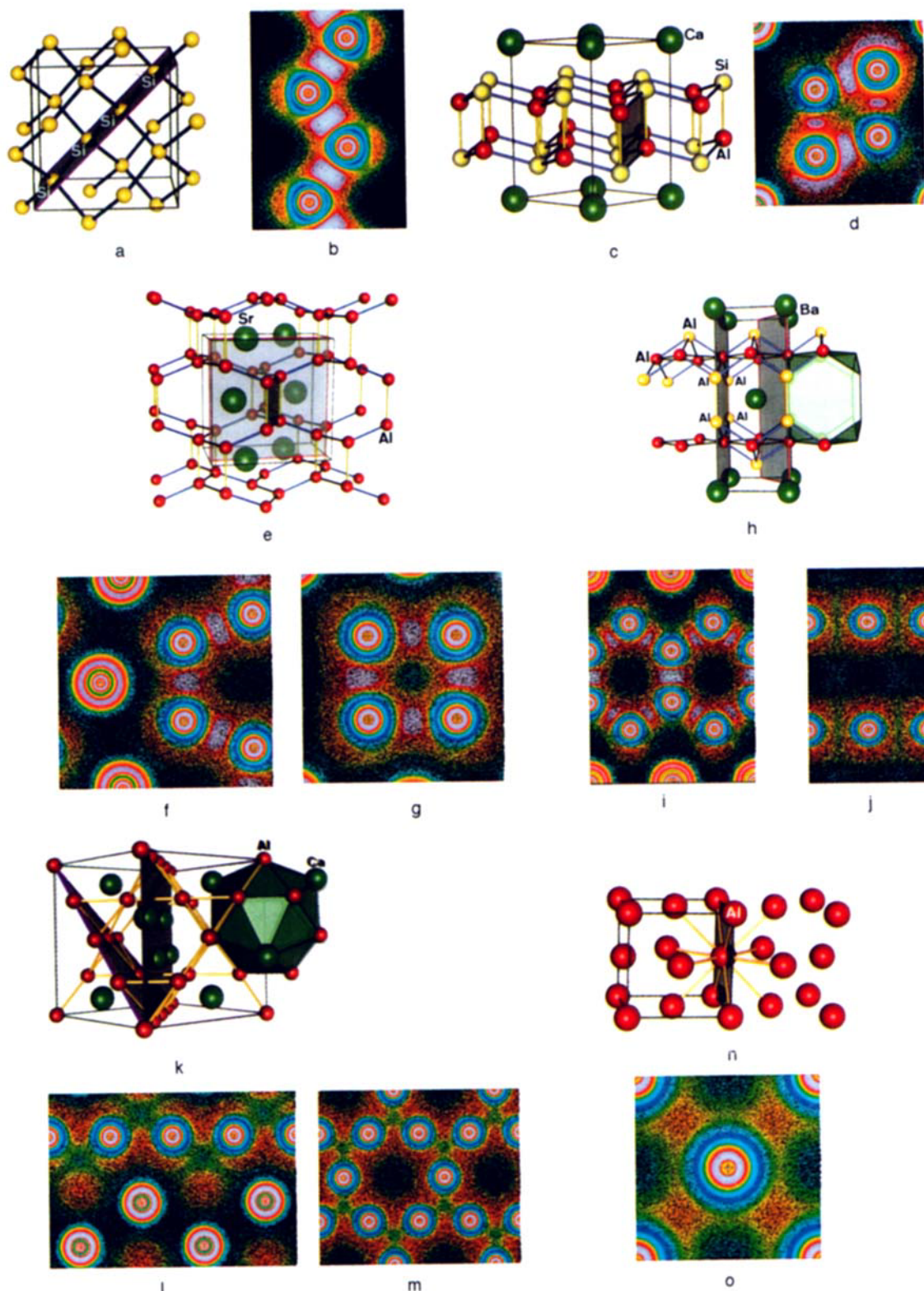
Figure 12. Structure and ELF representations (based on LMTO calculations) of selected 2D cross sections of the following structures: a), b) α-silicon, c), d) CaAl$_2$Si$_2$, e)–g) SrAl$_2$, h)–j) BaAl$_4$, k)–m) CaAl$_2$, n), o) α-Al. This series is representative for the transition from valence compounds to metals.

tion schemes and as such lead to different results. In principle, centers which are meaningful in structural chemistry, such as the so-called attractors (molecules, complexes, atoms, centers of bonds, etc.) and their domains (WBs) are defined.[21, 85] The most basic model is that of rigid spheres that do not completely fill the space. The simplest, and for the most part volume-pre-

serving domain (WB) division was proposed by Voronoi and Dirichlet[86] in the 19th century and used by Niggli and Laves for crystal chemical investigations.[87, 88] The domains (WB) are restricted by the construction of convex polyhedra around the attractors. A sufficient number of planes are erected on the interatomic vectors so that the polyhedra are completely

closed. The division point on the vector can be chosen according to radius relation criteria and is critical. Even the volume-preserving power plane method[89] is not free from that arbitrariness. Furthermore, the restriction of domains (WBs) by planes is a relatively rough approximation.

As mentioned, domains (WBs) of single atoms or ions are obtained upon the division of electron density according to the method of Bader.[12] A corresponding division with ELF yields electronic domains (WBs) for atom cores (only in the case of all-electron calculations), lone pair electrons, bonds, and bonding contributions such as in cluster compounds with delocalized three-center bonds (e.g. boranes). Both the atomic and electronic domains (WBs) can be used for integration of incremental values such as partial charges, ionicity of bonds, and number of electrons per interaction center per attractor.

The domain (WB) regions for the electron density in α-Al, α-Si, and $CaAl_2$ in the form of three-dimensional envelopes are shown in Figures 13a, c, and g, respectively. Whereas a euclidean polyhedron (rhombic dodecahedron) is obtained for aluminum, the border planes for the atomic cells of α-Si and $CaAl_2$ are bent. A comparison of the edges of the polyhedra for the euclidean division (Figure 13f) and the division of orthogonal trajectories according to Bader[12] (Figure 13e) clearly reveals different results due to the restriction to planar borders in the former case.
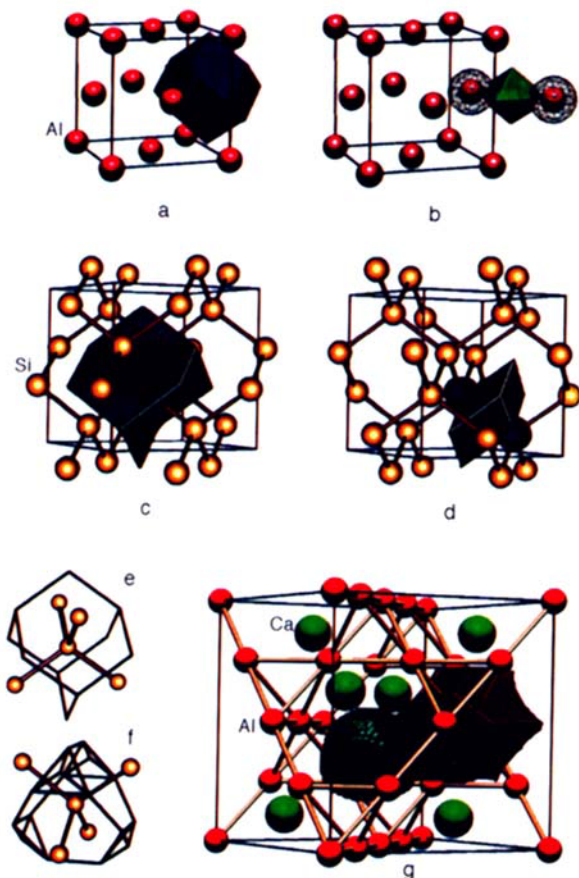
The clearly structured domain (WB) of Al in $CaAl_2$ is striking (red) (Figure 13g). It appears to be polarized by an almost spherical core region around Ca (green). This implies that significant ionic bonding contributions are present in the $CaAl_2$ Laves phase as evidenced by a relatively hard cation ($Ca^{\delta+}$) and a very soft anion ($Al_{\frac{1}{2}}^{\delta-}$) and thus covalent Al–Al interactions may be assumed. The quantitative investigations confirm this impression convincingly (see Table 2). Figures 13b and d show the divisions for the corresponding ELF.

Figure 14 displays the course of the trajectories in the two-dimensional sections in Figure 12; each picture shows the division of the electron density (atomic regions, top) and the division of the ELF (electronic regions, bottom). A comparison of both regions reveals a certain duality in the sense that where attractors are found in ELF, trajectories are present in the electron density and a minimum is found for the electron density at bond critical points along the interatomic vector. Furthermore, in $CaAl_2Si_2$, $SrAl_2$, $BaAl_4$, and $CaAl_2$ only one attractor is found for the alkaline earth metals and it is at the core position. This

Figure 13. Domain (WB) divisions for quantitative partitioning of electron densities ρ [12] (a,c,g) and ELF (b,d). a),b) Al; c),d) Si; g) $CaAl_2$. The bonding regions in b) and d) appear either as a distorted octahedron (α-Al, green) or as a rhombus (α-Si, dark green). e) The atomic domain (WB) in α-Si may be described as a saddle polyhedron with bent boundary planes. The comparison of the topology of edges of this polyhedron with that obtained by a geometrical division method f) [89] reveals distinctive differences.
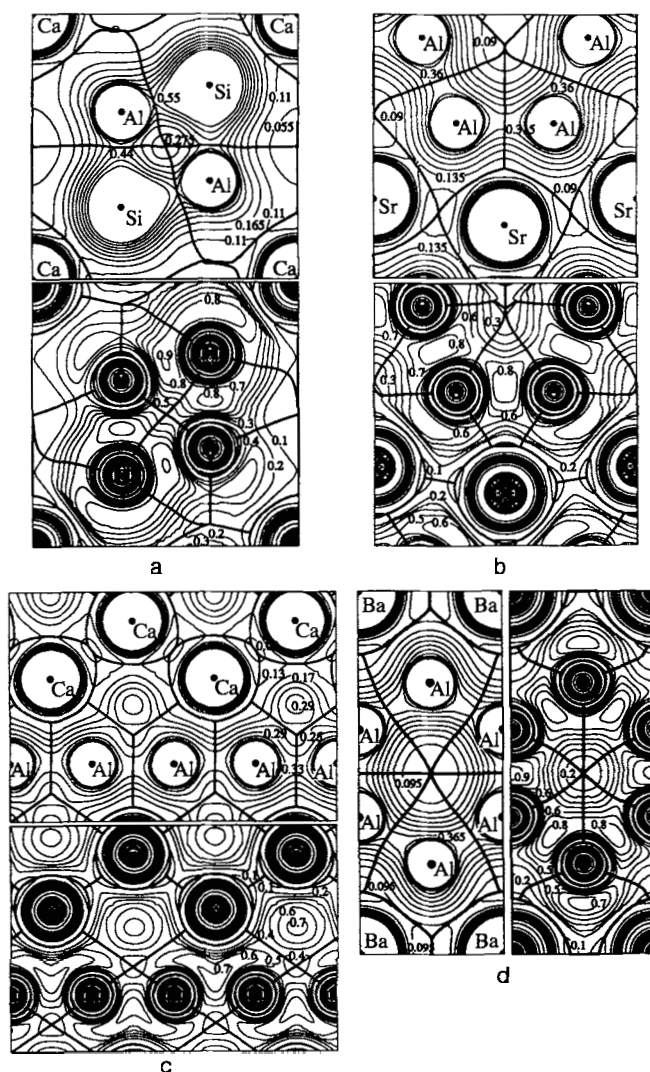

Figure 14. Contour line diagrams (thin black lines) with orthogonal trajectories that indicate the course of space divisions (thick black lines) in pairs for the electron density (top) and ELF (bottom) for a) $CaAl_2Si_2$, b) $SrAl_2$, c) $CaAl_2$, and d) $BaAl_4$ (LMTO calculations). The values given in Table 2 are obtained by separately integrating each domain (WB).

coincidence of atomic and electronic domains is indicative of the presence of quasi-ions in all cases. Furthermore, it is interesting that the domains (WB) in electron density and those of the cores in ELF are almost equal in form and extension for the electropositive metals Ca, Sr, and Ba. In Figure 14 these dual relations between ρ and ELF as well as the corelike form of the electronic domains at Ca, Sr, and Ba are emphasized.

Some quantitative values of this domain (WB) analysis are given in Table 2. The division of ρ yields partial charges q (difference between the number of valence electrons in the neutral atom and the N_e(at.) values) that are about the same with respect to the electropositive metals for the intermetallic phases $SrAl_2$ and $CaAl_2$ ($q(Ca) \approx q Sr) \approx 1$). Suprisingly, the charge does not increase in $BaAl_4$ ($q(Ba) \approx +0.7$) although the concentration of the more electronegative component Al is doubled. As expected the calcium atom in $CaAl_2Si_2$ carries a higher charge ($q(Ca) \approx +1.3$). However, the high positive charge of aluminum ($q(Al) \approx +1.3$) in this phase is unexpected. Actually, aluminum and silicon form a network with clearly covalent bonding contributions that are expressed in the ELF in the form of separable electronic attractors (see Figure 14a). The term "polar covalency" can be used to describe $CaAl_2Si_2$ with the formulation ($Ca^{\alpha+}[Al^{\beta+}Si^{\gamma-}]_2$), whereas the interaction between Ca centers and $[Al_2Si_2]$ has pronounced ionic character.

Table 2. Quantification of the electron density and the ELF over domain (WB) divisions: N_e(at.): Number of electrons for atomic domains (WB); N_e(al.): Number of electrons for electronic domain (WB) and ELF attractor.

Compound	atomic cell	N_e(at.)	electronic cell	N_e(el.)	distance [pm]
α-Al	Al atom	3.01	Al–Al	0.5	286.3
$CaAl_2$	Ca atom	0.99			
	Al atom	3.50	Al–Al	1.30	284.2
$SrAl_2$	Sr atom	1.01	Al–Al	2.13	279.9
	Al atom	3.51	Al–Al	2.01	278.6
			Al–Al	1.60	293.0
$BaAl_4$	Ba atom	1.33	Al–Al	2.05	278.4
	Al atom	2.57	Al–Al	1.45	272.5
	Al atom	3.75	Al–Al	-	305.2
$CaAl_2Si_2$	Ca atom	0.77	e_2-pair	1.96	
	Al atom	1.46	Al–Si	1.67	248.9
	Si atom	6.18	Al–Al	1.00	257.2
α-Si	Si atom	4.03	Si–Si	2.02	235.1

The effective electron numbers per domain (WB) reveal the influence of the corresponding attractor (bond, formula unit). Domain (WB) regions with approximately two electrons include the Si–Si bond, one of the three kinds of Al–Al bonds in $SrAl_2$, as well as the lone pair in $CaAl_2Si_2$ (Table 2). The integration of another Al–Al bond in $SrAl_2$ yields slightly more than two electrons; the cross section through this bond shows an elliptic form of the ELF. A weak π-bonding contribution seems to be present, but it does not appear to influence the bond length. Similar effects have also been found in Zintl anions of silicon.[31, 74, 75, 81] Smaller integrated electron numbers indicate multicenter bonds (see $BaAl_4$) or polar bonds with a corresponding Coulomb contribution.

The quantitative results summarized here reveal ELF to be very suitable for the examination of intermetallic phases. The

function is particularly valuable because the rules of valency do not hold here and there is no other comprehensive bonding theory yet. However, according to the few ELF investigations to date it is evident that the exceptional feature of intermetallic phases is a mixture of a wide variety of bonding forms.

4.3. $CuAl_2$ and Its Variants

The $CuAl_2$ structure is the aristo structure type of a great number of intermetallic phases. Pt_3Ga_7, $PdSn_3$, $PtSn_4$, $PtPb_4$, $RhBi_4$, and $PdGa_5$ are isotypical to or derived from the $CuAl_2$ structure. All these compounds can be classified under type B (see Section 4). They feature a common building element, namely square antiprisms of main group elements E, which are interconnected[92, 93] in various ways through E–E, T–E, and T–T bonds (T = transition element). Examination of the local chemical bond with ELF reveals the development of totally different, strongly bound partial fragments especially in the E partial structure,[95] which are accompanied by a noticeable localization within the square antiprisms. In $CuAl_2$, for example, there are strong bonds between the Al pairs connecting the prisms.[96] This is reminiscent of the strong bonds between boron polyhedra and the terminal two-electron–two-center bonds in boron clusters, and of the Ga_2 pairs in the structure of α-Ga.[94] These bonds are sections of two interpenetrating graphite-like networks.[96]

The lone pairs of electrons in $PtPb_4$ and $RhBi_4$ are located on the main group elements that are oriented according to the topology of simple periodical nodal surfaces (PNSs).[95, 97] Such a surface-active behavior of inert pairs of electrons is known, for example, from the work of Andersson, Galy et al.,[98] and has also been interpreted by using PNS.[99] In $PdGa_5$, the Ga_4 squares emerge as the more strongly bound units and, according to quantitative analyses, four electrons (i.e. two bonds) are distributed over the four-membered groups.[95] Furthermore, weak Pd–Ga interactions were found described in the sense of a "real" metallic bond. It was shown here that different interactions are spatially separated and that this division can be simply visualized with the aid of a PNS.[95]

5. ELF of Surfaces

The surface structures of many substances are unknown today. The reconstruction and passivation of surfaces are crucial phenomena that determine, for example, reactivity, thermal stability, crystal growth, electrolytical, and sintering characteristics. With regard to the specific control of these phenomena and to the access to nanotechnology, mechanistic bonding and dynamic models become extremely important, particularly because the surface area becomes more important as the particles become smaller.

Scanning probe methods enable exciting new insights in surface phenomena, and with scanning tunnel microscopy (STM) it is possible to generate images of surfaces at subatomic resolution. The corresponding images cannot easily be interpreted, because they depend on many factors such as composition of the probe tip, surface covering, bias voltage, and the density of

Angew. Chem. Int. Ed. Engl. **1997**, *36*, 1808–1832

1825

states close to the Fermi level for the surface.[100] The latter means that only a part of the electronic structure of the surface is explored. For this reason it is interesting to carry out theoretical modeling of surfaces not only with calculations of partial electron densities (PED) alone but also with the ELF. Spatial representations that may also be calculated for surfaces are obtained with both methods and both are able to reproduce aspects of STM images.

Today, surfaces of silicon single crystals are among the most well defined and thoroughly examined surfaces. The (100) surface of silicon has been frequently and controversially discussed. It is known that a 2×1 surface reconstruction takes place, but there is no agreement as to whether the dimer formation is symmetrical or unsymmetrical (Figure 15a).[101, 102] The results of the theoretical investigations depend on the quality of the calculation and there is no consensus yet as to which model is superior. However, it is possible to draw direct topological comparisons between experiment and models with the PED and the ELF. Figure 15b shows the corresponding density of states (DOS) close to the Fermi level (E_F) of the three surface situations depicted in Figure 15a. It is clearly seen that in both cases the reconstruction (formation of dimer) leads to a decrease of the DOS at E_F. Figure 15c reveals the total valence electron densities (TEDs, top), the partial electron densities (PEDs) for unoccupied states ($E_F \leq E \leq (E_F + 3 \text{ eV})$ center), and the PED for occupied states close to E_F ($(E_F - 3 \text{ eV}) \leq E \leq E_F$, bottom) for the same three situations. The accompanying 2D ELF cross sections calculations are presented in Figure 15d for quantum mechanical states occupied up to $E_F + 3$ eV (top) and for the states occupied up to E_F (bottom). Figure 15e shows the accompanying three-dimensional isosurface representations of ELF, whose exact form depends on the ELF value. Since ELF is always determined over all occupied states, the images obtained from the detection of the unoccupied (virtual) states (tunnel current from the tip to the surface) and occupied states (reversed tunnel current) must be simulated with the calculation of a slightly reduced or neutral system (Figure 15e bottom).

The comparison of calculated images with those measured (Figures 15f and g) for both directions of bias voltage shows interesting differences, which are discussed in reference [101]. Figure 15f shows the STM picture at positive bias voltage (electrons move from the tip to the surface) and therefore a reproduction of the unoccupied states (conduction band) of the surface.[103] This corresponds to Figures 15c center, 15d top, and 15e top. The result for the reversed bias voltage (electrons move from the surface to the tip) is presented in Figure 15g. The correlation to the calculated Figures 15c bottom, 15d bottom, and 15e bottom is clear.

At this point it must be stressed that

1. the TED is not sufficiently structured for a good explanation of these observations,
2. the PED are well structured and subtly differentiable but change significantly with small variations of the energy window [$(E_F - \Delta E)$, E_F] (like the STM pictures upon change of the bias voltage),
3. the ELF shows a situation intermediate to TED and the PED, that is it is well structured and considers all occupied states.

The advantage of ELF is that it not only provides an accurate reproduction of the spatial distribution but also a detailed image of the chemical bond and, particularly here, of dangling bonds at the surface. This is rarely possible with the other methods. Therefore ELF provides necessary and sufficient information for the analysis of STM images. It must be emphasized that there is no theoretical basis up to now for a relation between ELF and the STM experiment.

6. Localization Patterns in Interstitial Space

Nowadays, diffraction methods constitute a most important part of the determination of structure–property relationships. However, in some cases X-ray diffraction methods face nontrivial problems if, for example, super- or noncommensurate structures are to be determined, if twinning or disorder phenomena demand very sophisticated approaches, or if very light atoms must be resolved in the presence of strong X-ray scatterers.

Semiconducting compounds such as Zintl phases can in general be rationalized by the application of simple bonding concepts.[104] If, however, unusual or unexpected moieties occur it is not always certain whether they actually exist or are just an artifact of an erroneous structure determination.[105, 106] The existence of a geometrical void in such a structure is expected to arouse suspicion, but it cannot be used as a sure indicator for an overlooked atom or group of atoms. The "free" space may be generated for electronic reasons, for example as a packing space for lone pairs that are tightly bound to specific atoms, or of more or less free electrons as in electrides, intermetallic compoundss, and metals. The ELF is an extraordinarily useful sensor, especially for such problems in structure determination.[107]

Several times we have alluded to hierarchical relations in the sense that an ELF attractor also represents electrophilic particles such as protons. Mostly, these special attractors can be assigned to a part of the atomic structure. We should point out that ELF enables the visualization of patterns in interstitial space in such regions that cannot be associated with single atoms. The following four examples illustrate that such patterns, which indicate weakly bound but still spatially localized electrons, are in many cases indicative of overlooked atoms and thus may be of considerable importance for verifying the correctness of a structure.

6.1. Suboxides of Zintl Phases

To corroborate our findings concerning ELF we analyzed with LMTO band structure calculations[36] Zintl phases that contain light heteroatoms X in addition to mononuclear and oligomeric Zintl anions.

Compound Ca_4Sb_2O[108] was first described as a binary calcium antimonide Ca_2Sb[109] (Figure 16a), an assertion corrected shortly thereafter by the authors. The structure contains isolated Sb^{3-} ions and thus the compound can only be a valence compound, as expected, if an additional X^{2-} anion is present. The additional anion was identified as O^{2-} coordinated octahedrally by six calcium atoms. Surprisingly, the calculation of the ELF for Ca_4Sb_2 (without the O atom!) generates one and only
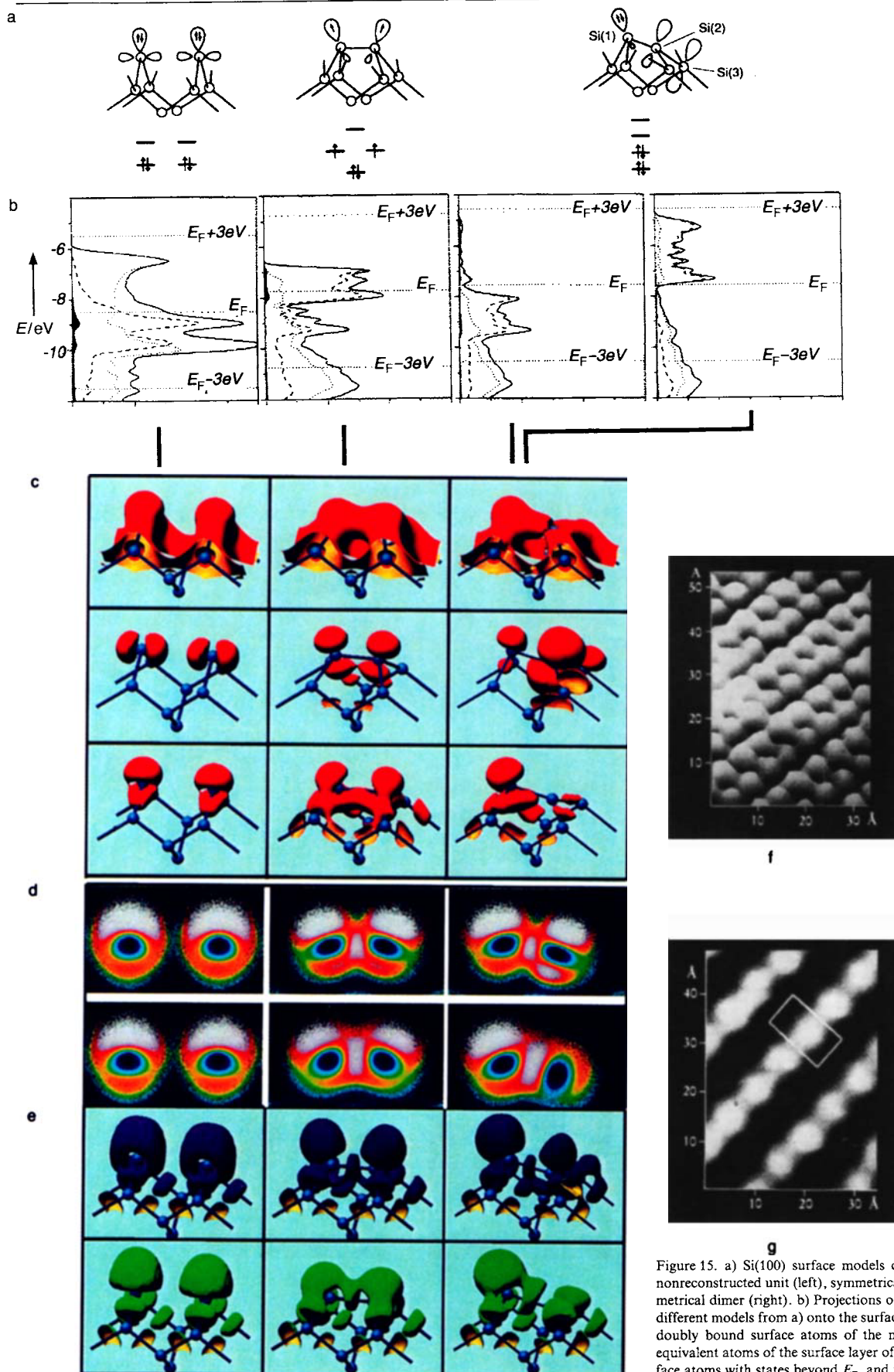
Figure 15. a) Si(100) surface models containing dangling bonds: nonreconstructed unit (left), symmetrical dimer (center), and asymmetrical dimer (right). b) Projections of the density of states of the different models from a) onto the surface atoms. From left to right: doubly bound surface atoms of the nonreconstructed unit, both equivalent atoms of the surface layer of the symmetrical dimer, surface atoms with states beyond E_F, and the atoms slightly below the surface with states above E_F. c) 3D representations of isosurfaces of TED (top row), PED of states in the energy region from E_F to $E_F + 3$ eV (second row), and PED in the region from $E_F - 3$ eV to E_F (third row). d) and e) 2D and 3D representations, respectively, of ELF with electronic occupation up to E_F (corresponding to the electron number of Si, bottom row), and with electronic occupation of the states up to $E_F + 3$ eV (corresponding to the formation of a further electron pair at the surface atoms, top row). f) STM image of the unoccupied surface states (positive bias voltage). g) STM image of the occupied surface states (negative bias voltage).
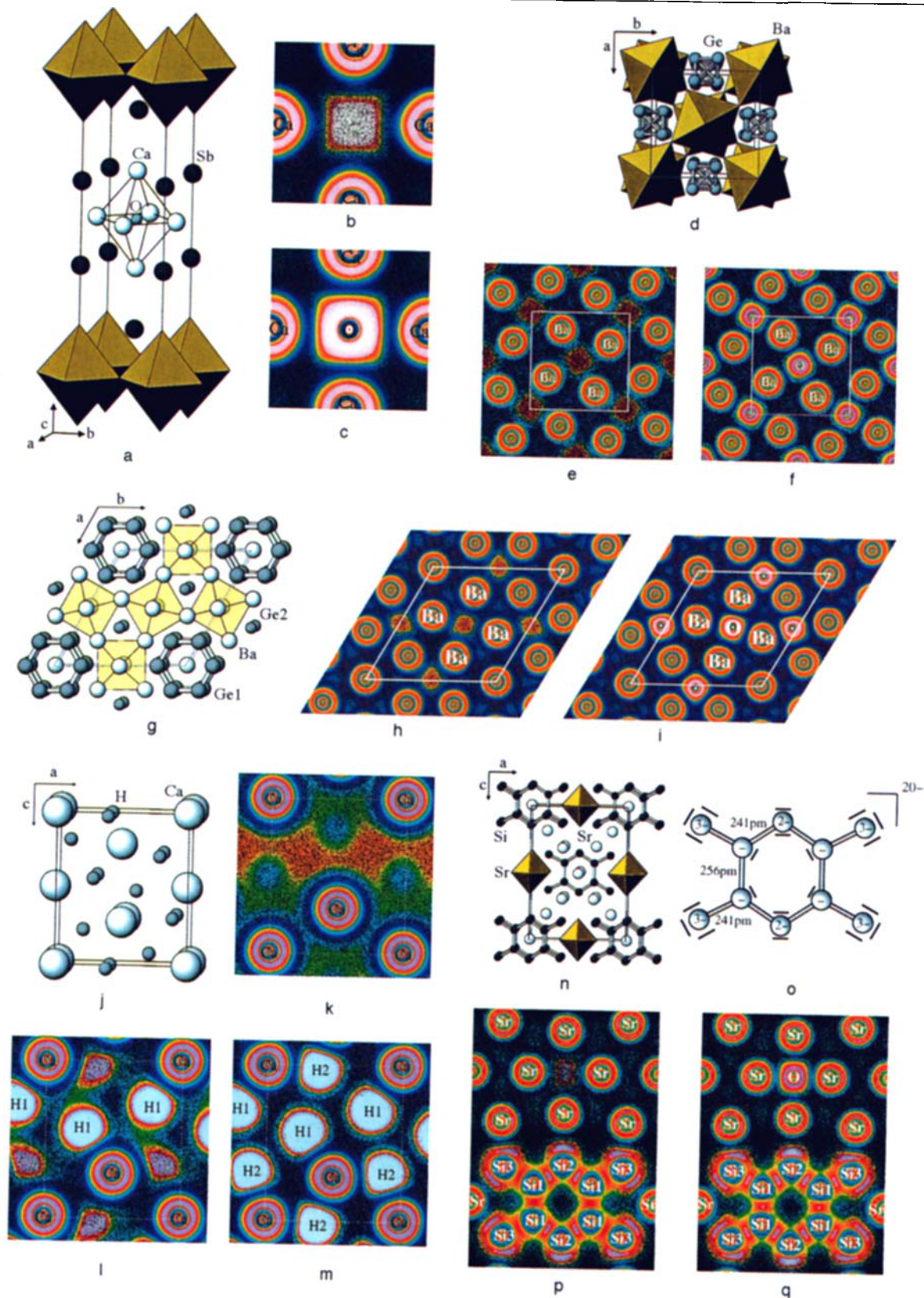
Figure 16. Structures and representative ELF (LMTO) cross sections with and without interstitial atoms (see text): a) structure of Ca_4Sb_2O, b), c) cross sections of the empty Sr_6 octahedron (ELF of the empty octahedron suggests the presence of the heteroatom) and with interstitial O atom, respectively; d) structure of Ba_3Ge_4X, e), f) cross sections of the empty Ba_6 octahedron and with interstitial O atom, respectively; g) structure of $Ba_3Ge_7O_3$ h), i) cross sections of the empty Ba_6 octahedron and with interstitial O atom, respectively; j) structure of CaH_2, k)–m) ELF of the Ca partial structure, with only one crystallographically unique H atom, and with all H atoms, respectively; n)–q) "SrSi" (second modification), n) structure with empty Sr octahedra [79], o) planar Zintl anion $[Si_{10}]^{(20-x)-}$, p) ELF cross section containing a Si_{10} unit and a Sr_6 octahedra; q) like p) but with O as a heteroatom corresponding to the $Sr_{10}Si_{10}O$ composition.

one additional localization region, which lies at the center of the Ca_6 octahedron (Figure 16b, white area). After introduction of the O atom into the calculation, an ELF is yielded that clearly displays the O atom with its core regions (Figure 16c). It is remarkable that despite the use of the different electron counts similar localization patterns are found for Ca_4Sb_2 ($\{8 + 10\}e$) and Ca_4Sb_2O ($\{8 + 10 + 6\}e$).

Quite recently, von Schnering et al. synthesized derivatives of barium germanides that contain Ba_6X octahedra and typical Zintl anions of germanium.[110, 111] In Ba_3Ge_4X there are Ge_4^{4-} tetrahedra (Figure 16d) and in $Ba_{10}Ge_7X$ planar Ge_6^{10-} rings occur. The ELF distributions without the heteroatoms X show localization patterns that are exactly at those positions that are occupied by X atoms or X groups. Figures 16e,f,h,i display the corresponding ELF sections through the Ba_6 octahedra without (Figures 16e,h) and with the X atoms (Figures 16f,i, X = O). The ELF displays the sites of the heteroatoms quite convincingly. According to the Zintl–Klemm concept and band structure calculations, X^{2-} units such as O^{2-}, C_2^{2-}, NH^{2-} are expected in these sites.[112]

The so-called second modification of "SrSi" (Figure 16n), which has never been confirmed experimentally, contains a very interesting Zintl anion, a planar $[Si_{10}]^{20-}$ unit with quite a peculiar variation in Si–Si bond lengths.[113] One would expect a formal charge distribution for this Zintl anion like that depicted Figure 16o. However, the Si1–Si1 bond lengths (256 pm) are so much longer than the other two (Si1–Si2 241 pm, Si1–Si3 241 pm) that this explanation seems quite suspect. A closer inspection reveals that the Sr atoms form an empty octahedron. The ELF treatment reveals a localization pattern (white spots in the structural section in Figure 16p) consistent with the assumption of σ bonds between Si1 and Si2. The lone pairs are indicated by white clouds of high ELF value located at expected positions.

The long Si1–Si1 bond has unusually low ELF values. More remarkable, however, is the center of the single Si1–Si3 bond (241 pm), for which a white region is to be expected, if the electron structure shows no peculiarities, and thus obeys the Zintl–Klemm concept (Figure 16o).[104]

Even more surprising is the large localization region between the four Sr atoms in the upper middle of Figure 16p. Two additional Sr atoms above and below that plane generate a distorted octahedron that shows a remarkable contraction compared with the neighboring Sr groups on the left and right side. Too high an accumulation of charge on the Zintl anion could lead to the formation of a cage orbital[106] in the Sr_6 octahedron. In this case, SrSi would belong to the class of electrides. The center of the octahedron, however, is an ideal position for an electronegative heteroatom such as oxygen. The corresponding distances (4×245, 2×285 pm) coincide very well with the Sr–O distances found in SrO (6×257 pm, ref. [114]) and in $SrTiO_3$ (12×276 pm, ref. [115]). The presence of a heteroatom would also explain the failed attempts to synthesize this "SrSi" modification from rigorously purified elements.[116] Neither the EH nor the LMTO investigations on the hypothetical phase $Sr_{10}Si_{10}O$ reveal a band gap at the Fermi level indicating a semiconductor. Therefore, there is no preferred valence electron number that allows for the more electronegative neighbors of oxygen, such as fluorine, nitrogen, or carbon, to act as heteroatoms.[117] In the

meantime, it has been shown on numerous Zintl phases that a limited capacity for accumulation of charge in highly charged Zintl anions leads to a planar geometry and a partially occupied π system. For the binary "SrSi", there are unusually high Sr contributions to a few bands below the Fermi level. This is quite unusual according to our experience.

A LMTO calculation with oxygen in the void position leads to an ELF that shows a surprisingly smooth distribution of white bond regions in the Si_{10} framework (Figure 16q), and the Sr contribution below the Fermi level disappears. We would like to emphasize that it was not obvious at the outset that a removal of two electrons from the Si partial structure to the O^{2-} ion would generate a, by our standards, very reasonable σ-bonded structure that is understandable with the quantum mechanical ELF analysis.

6.2. Determination of Hydrogen Positions in Hydrides

The following example, CaH_2,[119, 120] is important because, in general, hydrides present a problem in structure determination. Quite frequently, such compounds are microcrystalline and thus single-crystal investigations cannot be performed. Furthermore, hydride positions may not be found by X-ray analysis because of the small scattering factor of hydrogen.

To follow the typical procedure adopted in the determination of a hydride structure, the CaH_2 structure was analyzed with the ELF starting with the pure Ca substructure. Figures 16j—m display a section of the structure that contains atom positions Ca, H1, and H2. In Figure 16k the ELF is shown for the pure Ca substructure, that is without electron pair acceptors. There is a weak but significant localization (yellow spot) that includes the position of H2. If now one H atom is added and located at that site, a new localization spot that coincides with the position of H1 becomes clearly visible (Figure 16l). Actually this second localization region is already distinct in the ELF for the Ca substructure, but only equally as strong as a neighboring position unoccupied by H. These two weaker localization regions can be clearly distinguished after an antisymmetrical introduction of the first H atom on the observed position.[119] Therefore, this second localization region is clearly observable in a subsequent ELF calculation (Figure 16l).

The ELF of the complete structure (Figure 16m) beautifully reveals the ionic character of this hydride: there are only low ELF minima between the atoms. Nevertheless, a significant polarization is visible, especially of the hydride ions but also of the Ca^{2+} ions, which includes deviations from the spherical symmetry.

We must emphasize that this new way for the determination of missing atom positions is less reliable if the substructure reveals a higher symmetry than the complete structure, because the quantum mechanical calculation represents only a given symmetry. For example, starting from the magnesium position in MgH_2, an isolated localization cloud is obtained that indicates an interstitial region.[21, 31] But this region only represents the center of a region containing two hydride ions and does not permit any further geometrical specifications. Starting with such information, further methods in optimizing geometry can successfully lead to a complete structural model.

There are many indications that ELF describes the chemical bond in molecules, clusters, and extended structures in such a differentiated way, that, in general, regions of high ELF values can be understood as nucleophilic centers. With ELF it is possible to find missing atoms in incomplete structures, and in fact, as in CaH_2, even the positions of the major component and not only of a few of overlooked atoms.

7. Outlook

7.1. The Chemical Bond in Intermetallic Phases

Quite recently, a highlight by J. C. Schön appeared in this journal dealing with the chemical bond.[90] Therein an article by Burdett et al.,[91] and especially the following statement, was critically discussed: "...that the 'metallic bond' as a separate term with equal weight to the other three traditional schemes[*] should be abandoned" and "certainly it does not have a mathematical framework distinct from the other three categories...". Equivalently, the metallic bond does not represent a special type of chemical bond because previously known bonding types appear simultaneously in the corresponding structures and band structures should be used in the classification.[91] The rebuttal of Schön praised the usefulness of the usual forms of description of the metallic bond and criticized Burdett et al. for focussing on only one method (EH) for the calculation of band structures.

We believe that both authors are certainly correct, but the essential things that are governed by the term metallic bond are not yet fully understood. In our ELF investigations on intermetallic phases, definite localized bonding structures are found, mostly coexisting with ionic interactions, two-electron–two-center, two-electron–three-center, multielectron–multicenter bonds, as well as lone pair electrons, and conducting electrons. Here, clear separations between bonding forms, as known from valence compounds, can no longer be drawn. Furthermore, intermetallic phases sometimes show a very complicated structural chemistry. This proves that the coexistence of totally different bonding forms leads to a new structure chemical quality, where local and cooperative effects arrange themselves in very specific ways. The metallic bond might be one of the most homogeneous of all bonding classes with respect to differences in localization, but at the same time one of the most complex regarding the variety of bonding forms that are simultaneously present in a structure.

Evidently, the metallic bond may be explained by using a combination of classical bonding concepts but there is no reason to reject its definition as an independent class. It is important that an independent phenomenon is described here that is valid for many substances. The essence of a system is not simply the sum of its parts. We believe that the essence of the characteristic features of metals and intermetallic phases as an independent class is not yet clear, but ELF will contribute significantly to this end.

7.2. Hierarchy

A totally general relation in the construction of chemical and presumably all other structures emerged from the analysis of the chemical bond with the aid of ELF: there is a hierarchical correlation between structures of equal basic topology. For example, there is a correlation between the structures of diamond, cristobalite, and $Li_{10}P_4N_{10}$.[120] Every C atom in the diamond structure is substituted by a SiO_4 tetrahedron in cristobalite and by a $P_4N_{10}^{10-}$ unit in $Li_{10}P_4N_{10}$. It is important here that the correlated structures belong to the same symmetry group or correspond to group–subgroup relations. The central sites, the positions of the C atoms in the diamond structure, are invariant attractors, whereas other structural elements are located at those sites in each of the accompanying structures. The chemical correlation between the building groups may change completely, but the topology of the structure invariant attractors (the center of gravity of the structure elements) is always preserved. In the mathematical sense, it is unimportant whether distortions of the complete structure (e.g. change of the angles, change of unit cell dimensions) occur as long as the number of principle neighbors around each invariant attractor remains unchanged.

Von Schnering has demonstrated "hierarchical relationships" in a great number of such hierarchical families.[121] Now, with the aid of ELF, localization regions of electrons may be introduced in such hierarchical relationships and thereby, surprising new correlations have been found. It seems that attractor structures, which are obtained from electron distributions using ELF, are also formed by atoms, molecules, or clusters. This was already demonstrated in individual cases, for example the attachment of hydrogen atoms at attractors of transition metal complexes and boranes (see Section 2.4).

This correlation seems to be most important for the structural relations of intermetallic phases, oxides, and fluorides found by O'Keeffe and Hyde.[122] In many cases the atomic distribution in intermetallic phases is identical or very similar to the cation distribution in oxides and fluorides. In 1991, one of us pointed at the misinterpretation of this correlation by O'Keeffe and Hyde, namely in the sense of large cations.[82] At the time an explanation was given correlating the electronic domains in intermetallic phases with the anion positions of oxides and fluorides.[82] So far, ELF investigations increasingly confirm this assumption and its unexpected scope. It seems that there are correlations between localization regions of electrons and many atomic or molecular structures. Further systematic investigations are necessary for the confirmation of this statement. We were surprised that this method can be reversed for the localization of missing atoms in uncompletely determined structures.

Such correlations have been occasionally observed[121, 123, 124] but not yet amalgamated into a general concept. The calculation of the ELF may be quite useful for a classification of this kind.[121] In this respect, the observed ELF patterns provide not only compound- or structure-specific information but gain a general topological significance.

_____
[*] This refers to ionic, covalent, and van der Waals bonding.

1830

Angew. Chem. Int. Ed. Engl. **1997**, *36*, 1808–1832

[1] R. J. Gillespie, R. S. Nyholm, *Q. Rev. Chem. Soc.* **1957**, *11*, 339; R. J. Gillespie, *Molecular Geometry*, Van Nostrand Reinhold, London, **1972**.

[2] K. Artmann, *Z. Naturforsch.* **1946**, *1*, 426.

[3] R. Daudel, *Quantum Theory of the Chemical Bond*, Reidel, Dordrecht, **1974**.

[4] A. Kossel, *Ann. Phys. Chem.* **1916**, *49*, 229.

[5] W. England, L. S. Salmon, K. Ruedenberg, *Fortschr. Chem. Forsch.* **1971**, *23*, 31; W. England, *Int. J. Quantum Chem.* **1971**, *5*, 683.

[6] R. S. Mulliken, *J. Chem. Phys.* **1955**, *23*, 1833, 1841, 2338, 2343.

[7] E. R. Davidson, *J. Chem. Phys.* **1967**, *46*, 3320.

[8] R. Ahlrichs, C. Erhard, *Chem. Unserer Zeit* **1985**, *19*, 120; R. Heinzmann, R. Ahlrichs, *Theor. Chim. Acta* **1976**, *42*, 33.

[9] J. E. Carpenter, F. Weinhold, *J. Mol. Struct.* **1988**, *169*, 411.

[10] R. Daudel, citation 12 in reference[11].

[11] K. Ruedenberg, W. H. E. Schwarz, *J. Chem. Phys.* **1990**, *92*, 4956.

[12] R. W. F. Bader, *Atoms in Molecules: A Quantum Theory*, Oxford University Press, Oxford, **1990**; see R. F. W. Bader, P. L. A. Popelier, T. A. Keith, *Angew. Chem.* **1994**, *106*, 647; *Angew. Chem. Int. Ed. Engl.* **1994**, *33*, 620. A comparison of the topologies of $\nabla^2\rho$ and the ELF presented here in respect to a series of atomic interactions is found in: R. W. F. Bader, S. Johnson, T.-H. Tang, P. L. A. Popelier, *J. Phys. Chem.* **1996**, *100*, 15398.

[13] W. L. Luken, J. C. Culberson, *Int. J. Quantum Chem.* **1982**, *16*, 265.

[14] A. D. Becke, N. E. Edgecombe, *J. Chem. Phys.* **1990**, *92*, 5397.

[15] According to Equations (3) and (6) within a certain space of very low density, ELF may adapt high values that are physically meaningless. For example, in the Be atom ELF has the value one at $\rho \to 0$ ($r \to \infty$). Principally, these difficulties may be removed by the definition of an effective ELF' as $\{1 + [(C(\vec{r}) + \varepsilon)/C_h(\rho(\vec{r}))]^2\}^{-1}$, where $\varepsilon = 2.87 \times 10^{-5}$ is chosen so that for $\rho \le 10^{-3}$ bohr^{-1} ELF' adapts smaller values than 0.5. (to this see ref. [21]).

[16] T. F. Fässler, A. Savin, *Chem. Unserer Zeit* **1997**, *31*, 110.

[17] J. F. Dobson, *J. Chem. Phys.* **1991**, *94*, 4328.

[18] R. Thom, *Stabilité Structurelle et Morphogénèse*, Intereditions, Paris, **1972**.

[19] B. Silvi, A. Savin, *Nature* **1994**, *371*, 683.

[20] For similar examinations of electron density see: P. Mezey in *Reviews in Computational Chemistry, Vol. 1*, (Ed.: K. B. Lipkowitz, D. B. Boyd), VCH, Weinheim, **1990**.

[21] A. Savin, B Silvi, F. Colonna, *Can. J. Chem.* **1996**, *74*, 1088.

[22] M. Kohout, A. Savin, *Int. J. Quantum Chem.* **1996**, *60*, 875.

[23] A. Savin, 2nd International Conference on Inorganic Chemistry, Stuttgart, **1993**.

[24] F. Colonna, A. Savin, B. Silvi, unpublished results.

[25] A. Savin, O. Jepsen, J. Flad, O. K. Andersen, H. Preuss, H. G. von Schnering, *Angew. Chem.* **1992**, *104*, 187; *Angew. Chem. Int. Ed. Engl.* **1992**, *31*, 187.

[26] W. Kohn, L. Sham, *Phys. Rev.* **1965**, *A 140*, 1133.

[27] Y. Tal, R. W. F. Bader, *Int. J. Quantum Chem. Symp.* **1978**, *12*, 153; see also R. M. Dreizler, E. K. U. Gross, *Density Functional Theory: An Approach to the Quantum Many-Body Problem*, Springer, Berlin, **1990**, p. 15.

[28] R. G. Parr, W. Yang, *Annu. Rev. Phys. Chem.* **1995**, *46*, 701.

[29] M. Kohout, A. Savin, *J. Comp. Chem.* **1997**, in press.

[30] A. Burckhardt, U. Wedig, H. G. von Schnering, A. Savin, *Z. Anorg. Allg. Chem.* **1993**, *619*, 437.

[31] S. Wengert, PhD thesis, ETH, Zürich, **1997**.

[32] A. Savin, A. D. Becke, J. Flad, R. Nesper, H. Preuss, H. G. von Schnering, *Angew. Chem.* **1991**, *103*, 421; *Angew. Chem. Int. Ed. Engl.* **1991**, *30*, 409.

[33] All Extended-Hückel calculations in this article were carried out with the program MEH-MACC[34], which allows the calculation of electron localization function, total electron density (TED), and the partial electron density (PED) and their graphical two- and three-dimensional representation based on charge self-consistent Hückel parameters H_{ii}.

[34] U. Häussermann, R. Nesper, S. Wengert, T. F. Fässler, program MEH-MACC, modified extended-Hückel version based on the QCPE program EH-MACC [35] (inquiries to mehmacc@inorg.chem.ethz.ch).

[35] Program EHMACC: M.-H. Whangbo, M. Evain, T. Hughbanks, M. Kertesz, S. Wijeyesekera, C. Wilker, C. Zheng, R. Hoffmann, R. Hoffmann, unpublished results.

[36] TB-LMTO-ASA: tight-binding linear muffin-tin orbital in the atomic sphere approximation. Program TB-LMTO: M. van Schilfgarde, T. A. Paxton, O. Jepsen, O. K. Andersen, G. Krier, Max-Planck-Institut für Festkörperforschung, Stuttgart, **1994**, unpublished results. All TB-LMTO-ASA calculations based on the LDA approximation were carried out by the use of the exchange correlation potential according to Barth and Hedin [37]. The radii of the muffin-tin spheres and sometimes necessary hollow spheres E within the framework of the ASA approximation are determined according to the method described by Jepsen and Andersen [38].

[37] U. Barth, L. Hedin, *J. Phys. C* **1972**, *5*, 1629.

[38] O. Jepsen, O. K. Andersen, *Z. Phys. B* **1995**, *97*, 35.

[39] Program GRAPA: J. Flad, F.-X. Fraschio, B. Miehlich, Institut für Theoretische Chemie der Universität, Stuttgart, **1989**.

[40] D. Seebach, H. M. Bürger, D. A. Plattner, R. Nesper, T. Fässler, *Helv. Chim. Acta* **1993**, *76*, 2581.

[41] L. Pauling, *The Nature of the Chemical Bond*, 3rd ed., Cornell University Press, **1960**, 136.

[42] R. J. Gillespie, I. Hargittai, *VSEPR Model of Molecular Geometry*, Allyn and Barton, Boston, **1991**; R. J. Gillespie, E. A. Robinson, *Angew. Chem.* **1996**, *108* , 539; *Angew. Chem. Int. Ed. Engl.* **1996**, *35*, 495.

[43] Naturally, like the electron density, ELF shows the total symmetry of the corresponding unit in contrast to the popular formulation in textbooks using localized two-electron centers with bonding lines.

[44] The presence of a torus instead of three separate attractors in the isoelectronic XeF$_2$ molecule was previously pointed out by S. Andersen, *Acta Crystallogr. Sect. B* **1979**, *35*, 1321.

[45] A. Savin, H. J. Flad, O. Flad, H. W. Preuss, H. G. von Schnering, *Angew. Chem.* **1992**, *104*, 185; *Angew. Chem. Int. Ed. Engl.* **1992**, *31*, 187.

[46] W. Kutzelnigg, *Angew. Chem.* **1984**, *96*, 262; *Angew. Chem. Int. Ed. Engl.* **1984**, *23*, 272.

[47] M. Kohout, A. Savin, J. Flad, H.Preuss, H. G. von Schnering, *Computer Aided Innovation of New Materials II* (Ed.: M. Doyama), Elsevier, **1997**, 261.

[48] T. F. Fässler, R. Glaser, unpublished results.

[49] H. L. Schläfer, G. Gliemann, *Einführung in die Ligandenfeldtheorie*, 2nd ed., Akademische Verlagsanstalt, Wiesbaden, **1980**.

[50] A. Savin, unpublished results.

[51] M. Kaupp, *Chem. Ber.* **1996**, *129*, 527.

[52] T. F. Fässler, unpublished results.

[53] K. Wade, *Adv. Inorg. Radiochem.* **1976**, *18*, 1.

[54] J. E. Huheey, E. A. Keiter, R. L. Keiter, *Inorganic Chemistry: Principles of Structure and Reactivity*, 2nd ed., Walter de Gruyter, Berlin **1995**.

[55] W. Hönle, Yu. Grin, U. Wedig, M. Schulthess, H. G. von Schnering, R. Kellner, H. Binder, *J. Solid State Chem.*, in press.

[56] A. Simon, *Chem. Unserer Zeit* **1976**, *10*, 9.

[57] Yu. Grin, personal communication.

[58] P. von R. Schleyer, J. Kapp, *Chem. Phys. Lett.* **1996**, *255*, 363.

[59] A. Simon, H. G. von Schnering, H. Schäfer, *Z. Anorg. Allg. Chem.* **1967**, *355*, 295; *ibid.* **1967**, *355*, 311; H. Imoto, A. Simon, *Inorg. Chem.* **1982**, *21*, 308.

[60] A. N. Fitch, S. A. Barrett, B. Fender, A. Simon, *J. Chem. Soc. Dalton Trans.* **1972**, *4*, 501.

[61] R. Chevrel in *Superconducting Materials Sciences—Metallurgy, Fabrication and Application*, (Eds.: S. Foner, B. B. Schwarz), Chapter 10, Plenum Press, New York **1981**.

[62] H. Schäfer, H. G. von Schnering, *Z. Anorg. Allg. Chem.* **1967**, *353*, 281.

[63] E. Zeller, H. Beruda, H. Schmidbaur, *Inorg. Chem.* **1993**, *24*, 3203.

[64] P. Pyykkö, N. Runeberg, *J. Chem. Soc. Chem. Commun.* **1993**, *24*, 1812.

[65] M. N. Gluhovtsev, P. von R. Schleyer, A. Stein, *J. Phys. Chem.* **1993**, *97*, 5541.

[66] A. Burkardt, PhD thesis, Universität Stuttgart, **1992**.

[67] H. G. von Schnering, W. Hönle, *Chem. Rev.* **1988**, *88*, 243.

[68] H. G. von Schnering, U. Wedig, R. Nesper, L. Schröder, R. H. Cardoso Gil, W. Carrillo-Cabrera, "Einfache Muster in komplexen Strukturen" (Simple Models in Complex Structures), *Jahrbuch der Max-Planck-Gesellschaft* **1994**, p. 390.

[69] K. A. Soltntsev, Y. A. Buslaev, N. T. Kuznetsov, *Russ. J. Inorg. Chem.* **1988**, *31*, 633.

[70] A. M. Mebel, O. P. Charkin, K. A. Soltntsev, N. T. Kuznetsov, *Russ. J. Inorg. Chem.* **1988**, *31*, 2263.

[71] F. A. Cotton, X. Feng, M. Shang, W. A. Wojtczak, *Angew. Chem.* **1992**, *104*, 1117; *Angew. Chem. Int. Ed. Engl.* **1992**, *31*, 1050.

[72] L. Chen, F. A. Cotton, W. A. Wojtzak, *Angew. Chem.* **1995**, *107*, 2050; *Angew. Chem. Int. Ed. Engl.* **1995**, *34*, 1877.

[73] F. A. Cotton, J. Lu, M. Shang, W. A. Wojtczak, *J. Am. Chem. Soc.* **1994**, *116*, 4364.

[74] A. Currao, PhD thesis, ETH Zürich, **1995**.

[75] R. Nesper, A. Currao, S.Wengert in *Organosilicon Chemistry, Vol. II, From Molecules to Materials* (Eds.: N. Auner, P. Weis), VCH, Weinheim, **1995**, p. 469.

[76] R. Nesper, A. Currao, S. Wengert, unpublished results.

[77] R. Nesper, unpublished results.

[78] W. Rieger, E. Parthé, *Acta Crystallogr.* **1967**, *22*, 919.

[79] B. Eisenmann, H. Schäfer, K. Turban, *Z. Naturforsch. B* **1974**, *29*, 464.

[80] F. Merlo, M. L. Fornasini, *J. Less-Common Met.* **1967**, *13*, 603.

[81] A. Currao, J. Curda, R. Nesper, *Z. Anorg. Allg. Chem.* **1996**, *622*, 85.

[82] R. Nesper, *Angew. Chem.* **1991**, *103*, 805; *Angew. Chem. Int. Ed. Engl.* **1991**, *30*, 789.

[83] D. G. Pettifor, *Solid State Commun.* **1984**, *51*, 37; P. Villars, *J. Less-Common Met.* **1986**, *119*, 89; P. Villars, K. Girgis, F. Hulliger, *ibid.* **1982**, *42*, 89.

[84] U. Häussermann, S. Wengert, P. Hoffmann, A. Savin, O. Jepsen, R. Nesper, *Angew. Chem.* **1994**, *106*, 2147; *Angew. Chem. Int. Ed. Engl.* **1994**, *33*, 2069.

[85] U. Häussermann, S. Wengert, R. Nesper, *Angew. Chem.* **1994**, *106*, 2151; *Angew. Chem. Int. Ed. Engl.* **1994**, *33*, 2073.

[86] G. L. Dirichlet, *J. Reine Angew. Math.* **1850**, *40*, 216; G. F. Voronoi, *ibid.* **1908**, *134*, 198.

[87] P. Niggli, *Z. Kristallogr.* **1928**, *68*, 404.

[88] F. Laves, *Z. Kristallogr.* **1931**, *78*, 208.

[89] W. Fischer, E. Koch, E. Hellner, *New Jahrb. Mineral. Monatsh.* **1971**, 227.

[90] J. C. Schön, *Angew. Chem.* **1995**, *107*, 1183; *Angew. Chem. Int. Ed. Engl.* **1995**, *34*, 1081. See also the ensuing correspondence between L. C. Allen and J. K Burdett, and J. C. Schön (*Angew. Chem.* **1995**, *107*, 2157; *Angew. Chem. Int. Ed. Engl.* **1995**, *34*, 2003).

[91] L. C. Allen, J. F. Capitani, *J. Am. Chem. Soc.* **1994**, *116*, 8810; W. P. Anderson, J. K. Burdett, P. T. Czech, *ibid.* **1994**, *116*, 8808.

[92] K. Schubert, *Kristallstrukturen zweikomponentiger Phasen*, Springer, Berlin, **1964**.

[93] Yu. Grin,, U. Wedig, H. G. von Schnering, *Jahresbericht des Max-Planck-Institut für Festkörperforschung Stuttgart*, **1995**, I-73; Poster B 14 at the Symposium for Theoretical Chemistry, Loccum, **1995**.

[94] H. G. von Schnering, R. Nesper, *Acta Chem. Scand.* **1991**, *45*, 870.

[95] Yu. Grin, U. Wedig, F. Wagner, H. G. von Schnering, A. Savin, *J. Alloys Compd.* **1997**, *255*, 203.

[96] Yu. Grin, U. Wedig, H. G. von Schnering, Poster C29 at the European Solid State Conference in Montpellier.

[97] Yu. Grin, U. Wedig, H. G. von Schnering, *Angew. Chem.* **1995**, *107*, 1318; *Angew. Chem. Int. Ed. Engl.* **1995**, *34*, 1204.

[98] J. Galy, G. Meunier, S. Andresson, A. Åström, *J. Solid State Chem.* **1975**, *9*, 92.

[99] R. Nesper, Habilitation thesis, Universität Stuttgart, **1989**; M. Oehme, PhD thesis, Universität Stuttgart, **1989**.

[100] E. Tekman, S. Cirai, *Phys. Rev. B Condens. Matter* **1989**, *40*, 10286; J. Tersoff, D. R. Hamann, *Phys. Rev. Lett.* **1983**, *50*, 1998; J. Tersoff, *ibid.* **1986**, *57*, 440; M.-H. Whangbo, S. N. Magonov, *Adv. Mater.* **1994**, *6*, 355.

[101] T. F. Fässler, U. Häußermann, R. Nesper, *Chem. Eur. J.* **1995**, *1*, 625.

[102] See also : H. N. Waldenbrug, J. T. Yates, Jr., *Chem. Rev.* **1995**, *95*, 1689.

[103] H. Neddermeyer, *Chem. Unserer Zeit* **1992**, *26*, 18; R. Kliese, B. Rüttger, D. Badt, H. Neddermeyer, *Ultramicroscopy* **1992**, *42*, 824.

[104] E. Zintl, *Angew. Chem.* **1939**, *52*, 1; E. Zintl, G. Brauer, *Z. Phys. Chem. Abt. B* **1933**, *20*, 245; E. Zintl, W. Dullenkopf, *Z. Phys. Chem. Abt. A* **1931**, *154*, 1; *Z. Phys. Chem. Abt. B* **1932**, *16*, 183; W. Klemm, *FIAT Review of German Science, Naturforschunf und Medizine in Deutschland 1939–1946, Anorganische Chemie Teil IV*, *26*, 103; W. Klemm, *Trab. Reun. Int. React. Solidos 3rd* **1956**, *1*, 447; W. Klemm, *Proc. Chem. Soc. London* **1959**, 329; E. Mooser, W. B. Pearson, *Phys. Rev.* **1956**, *101*, 1608; E. Mooser, W. B. Pearson, in *Progress in Semiconductors, Vol. 5* (Eds.: G. A. Gibson, F. A. Kröger, R. E. Burgess), Heywood, London, **1960**, p. 103; W. Klemm, *Festkörperprobleme*, Vieweg, Braunschweig, **1963**; E. Busmann, *Z. Anorg. Allg. Chem.* **1961**, *313*, 90; H. Schäfer, *Angew. Chem.* **1973**, *85*, 742; *Angew. Chem. Int. Ed. Engl.* **1973**, *12*, 694.

[105] H. G. von Schnering, R. Nesper, J. Curda, K.-F. Tebbe; *Angew. Chem.* **1980**, *92*, 1070; *Angew. Chem. Int. Ed. Engl.* **1980**, *19*, 1033; M. C. Böhm, R.

Ramirez, R. Nesper, H. G. von Schnering, *Phys. Rev.* **1984**, *B30*, 4870; M. C. Böhm, R. Ramirez, R. Nesper, H. G. von Schnering, *Ber. Bunsen-Ges. Phys. Chem.* **1985**, *89*, 465.

[106] R. Ramirez, R. Nesper, H. G. von Schnering, M. C. Böhm, *J. Phys. Chem. Solids* **1987**, *48*, 51.

[107] R. Nesper, S. Wengert, *Chem. Eur. J.* **1997**, *3*, 985.

[108] B. Eisenmann, H. Limartha, H. Schäfer, H. A. Graf, *Z. Naturforsch. B* **1980**, *35*, 1518.

[109] B. Eisenmann, H. Schäfer, *Z. Naturforsch. B* **1974**, *29*, 13; C. Harmon, R. Marchand, P. L'Haridon, Y. Laurant, *Acta Crystallogr. Sect. B* **1974**, *31*, 427.

[110] H. G. von Schnering, M. Somer, J. Curda, personal communication.

[111] H. G. von Schnering, U. Bolle, J. Curda, K. Peters, W. Carrillo-Cabrera, M. Somer, M. Schultheiss, U. Wedig, *Angew. Chem.* **1996**, *108*, 1062; *Angew. Chem. Int. Ed. Engl.* **1996**, *35*, 984.

[112] In Ba_3Ge_4X a split position is found for X, which can be interpreted in terms of a disordered C_2^{2-}; H. G. von Schnering, personal communication. This may be possible according to the ELF calculated for Ba_3Ge_4, but, as expected, there is no indication of an atomic distribution of lower symmetry.

[113] B. Eisenmann, H. Schäfer, K. Turban, *Z. Naturforsch. B* **1974**, *29*, 464.

[114] W. Gerlach, *Z. Phys.* **1922**, *9*, 184; W. Primak, H. Kaufmann, R. Ward, *J. Am. Chem. Soc.* **1948**, *70*, 2043.

[115] H. D. Megaw, *Proc. Phys. Soc. London* **1948**, *58*, 133; J. Hutton, R. J. Nelmes, *Acta Crystallogr. Sect. A* **1981**, *37*, 916.

[116] A. Currao, R. Nesper, unpublished results.

[117] Experience shows that EH calculations overestimate band gaps, whereas these values are systematically underestimated by LMTO analyses. If both methods reveal no band gap, the material under study is most probably metallic.

[118] B. Bergsma, B. O. Loopstra, *Acta Crystallogr.* **1962**, *15*, 92.

[119] A. F. Andresen, A. J. Maeland, D. Slotfeld-Ellingsen, *J. Solid State Chem.* **1977**, *20*, 93.

[120] W. Schnick, U. Berger, *Angew. Chem.* **1991**, *103*, 857; *Angew. Chem. Int. Ed. Engl.* **1991**, *30*, 830.

[121] H. G. von Schnering has always searched for such structural chemical interrelations. He employed the term "hierarchical relation" in various respects in the nineties, see, for example, ref. [68]; W. Carrillo-Cabrera, N. Caroca-Canales, K. Peters, H. G. von Schnering, *Z. Anorg. Allg. Chem.* **1993**, *619*, 1556; W. Carrillo-Cabrera, N. Caroca-Canales, H. G. von Schnering, *ibid.* **1994**, *620*, 247; ref. [32].

[122] M. O'Keeffe, B. G. Hyde, *Struct. Bonding (Berlin)* **1985**, *61*, 77.

[123] A. F. Wells, *Structural Inorganic Chemistry*, Clarendon Press, Oxford, **1991**.

[124] B. G. Hyde, S. Andersson, *Inorganic Crystal Structures*, Wiley, New York, **1989**.

1832

Angew. Chem. Int. Ed. Engl. **1997**, *36*, 1808–1832